

AD A114981

ETI-CR-82-1075

(12)

Investigation Of Liquid Drop Impacts On Ceramics

FINAL REPORT

by
William F. Adler

May 1982

Submitted to the
Office of Naval Research
800 North Quinoy Street
Arlington, VA 22217

Reproduction in whole or in part is permitted for
any purpose of the United States Government.

This research was sponsored by the Office of Naval
Research under Contract N00014-76-C-0744 NR 032-885.

EFFECTS TECHNOLOGY, INC.
A Subsidiary of Flow General, Inc.
5383 Hollister Avenue
Santa Barbara, California 93111
(805) 964-9831

DTIC
ELECTE
MAY 28 1982
S A D

This document has been approved
for public release and sale; its
distribution is unlimited.

82 05 28 047

DTIC FILE COPY

UNCLASSIFIED

SECURITY CLASSIFICATION OF THIS PAGE (When Data Entered)

REPORT DOCUMENTATION PAGE		READ INSTRUCTIONS BEFORE COMPLETING FORM
1. REPORT NUMBER	2. GOVT ACCESSION NO. <i>AJ-A114981</i>	3. RECIPIENT'S CATALOG NUMBER
4. TITLE (and Subtitle) INVESTIGATION OF LIQUID DROP IMPACTS ON CERAMICS		5. TYPE OF REPORT & PERIOD COVERED Final 24 March 1976 - 31 May 1982
7. AUTHOR(s) W. F. Adler		6. PERFORMING ORG. REPORT NUMBER CR-82-1075
9. PERFORMING ORGANIZATION NAME AND ADDRESS Effects Technology, Inc. 5383 Hollister Avenue Santa Barbara, CA 93111		8. CONTRACT OR GRANT NUMBER(s) N00014-76-C-0744
11. CONTROLLING OFFICE NAME AND ADDRESS Office of Naval Research 800 North Quincy Street Arlington, VA 22217		10. PROGRAM ELEMENT, PROJECT, TASK AREA & WORK UNIT NUMBERS Project No. 471
14. MONITORING AGENCY NAME & ADDRESS (if different from Controlling Office)		12. REPORT DATE 31 May 1982
		13. NUMBER OF PAGES 95
		15. SECURITY CLASS. (of this report) Unclassified
		15a. DECLASSIFICATION DOWNGRADING SCHEDULE
16. DISTRIBUTION STATEMENT (of this Report) Approved for public release; distribution unlimited.		
17. DISTRIBUTION STATEMENT (of the abstract entered in Block 20, if different from Report)		
18. SUPPLEMENTARY NOTES		
19. KEY WORDS (Continue on reverse side if necessary and identify by block number) Water Drop Impingement, Rain Erosion, Radomes, Infrared-Transmitting Window Materials, Fracture, Fracture Toughness, Ceramics, Magnesium Oxide, Magnesium Aluminate Spinel, Zinc Sulfide, Zinc Selenide, Silica Mullite, Germania Mullite, Aluminum Nitride, Yttria Zirconia, Pyroceram, Germanate Glass, Soda Lime Glass, Borosilicate Glass, Fused Silica, Magnesium Fluoride:		
20. ABSTRACT (Continue on reverse side if necessary and identify by block number) - The initial objective for this effort was to obtain an understanding of the response of ceramic materials on a microstructural level when subjected to water drop impact conditions (rain erosion). Before this objective could be satisfied it was necessary to have a well-controlled experimental arrangement so that the observed material damage, especially for very minor surface disruptions, could be related to a well-defined loading condition. A significant portion of the effort was devoted to achieving this test condition. The current status of the		

DD FORM 1473
1 JAN 73

EDITION OF 1 NOV 65 IS OBSOLETE

UNCLASSIFIED

SECURITY CLASSIFICATION OF THIS PAGE (When Data Entered)

UNCLASSIFIED

SECURITY CLASSIFICATION OF THIS PAGE(When Data Entered)

liquid drop impact facility is such that highly reproducible, well-documented, spherical water drop impacts can be obtained routinely at impact velocities from 200 to over 1000 ms^{-1} . The diameter of the water drops at present can be varied from 1.7 to 3.3 mm. The impact angle can range conveniently from approximately 45° to normal incidence. The capability also exists for evaluating the influence of a continuous variation in the level of water drop distortion on the extent of the damage due to distorted compared with spherical drops. Thus, a reasonably extensive range of parameters pertaining to most aspects of water drop impingement in a flight environment now exists.

All of the materials investigations reported during the course of this program utilized nominal 2.2 mm spherical drops impacting at normal incidence. Detailed investigations of calcium fluoride, magnesium oxide, lithium fluoride, magnesium aluminate spinel, and zinc sulfide were undertaken. In addition polymethylmethacrylate was used to obtain information about the impact loading conditions. Due to the excellent water drop impacts which can be obtained in the liquid drop impact facility, the development of adequate surface finishing procedures, and the development of damage characterization procedures, the results reported in previous investigations on lithium fluoride, zinc sulfide, and polymethylmethacrylate were shown to be completely in error or inaccurate.

In order to relate the impact damage to material properties a selection of materials for which the material properties are reasonably well known was assembled. The extent of the water drop impact damage was estimated from the surface fractures produced by roughly equivalent impact conditions. This comparison indicates that it is quite difficult to impossible to establish the water drop impact resistance of ceramic materials from their conventionally measured material properties. The water drop impact resistance displays wide variations for materials with essentially similar material properties. More detailed investigations are required to determine if any universal material properties can be found which control the water drop impact resistance of ceramic materials.

The work accomplished during the course of this investigation has contributed to clarifying prior concepts of rain erosion damage in materials, has provided a basis for the analysis of water drop impact damage and erosion predictions, has demonstrated that the suggested correlations between water drop impact damage and material properties cannot be substantiated, has provided a consistent means for experimentally evaluating the water drop impact resistance of materials, and has generated an alternative means (nylon bead impacts) for obtaining water drop impact damage evaluations for actual components, for superposed thermal environments, and for an extended range of impact velocities. Rapid progress should now be made in understanding and predicting rain erosion damage in materials utilizing these accomplishments which have required a considerable amount of time and effort to reach their present stage of development.

UNCLASSIFIED

SECURITY CLASSIFICATION OF THIS PAGE(When Data Entered)

CR-82-1075

Investigation Of Liquid Drop Impacts On Ceramics

FINAL REPORT

by
William F. Adler

May 1982

This research was sponsored by the Office of Naval
Research under Contract N00014-76-C-0744 NR 032-565.

EFFECTS TECHNOLOGY, INC.
A Subsidiary of Flow General, Inc.
5383 Hollister Avenue
Santa Barbara, California 93111
(805) 964-9831



Accession For
NTIS GRASI
DTIC TAB
Unannounced
Justification
by
DTIC TAB
Available
A

Foreword

The primary emphasis in this program was the examination of the microstructural damage produced in materials due to water drop impacts. However, before this materials-oriented program could be productive it was necessary to have a way to generate reproducible, controlled, and well-documented water drop impact conditions. This requirement became an integral part of the program, and a sizable developmental effort was undertaken for this purpose, not by choice, but by necessity. Fortunately, through the contributions of a number of individuals at Effects Technology, Inc., the experimental capability for generating water drop impacts on ceramic materials with a broad range of strength levels has been successfully developed and through a continuing evolution of improvements in the experimental facility exceeds the maximum impact velocity initially required for moderate strength ceramics by a factor of two and one-half.

Over the last few years the water drop impact behavior of a variety of single crystal and polycrystalline ceramics have been documented. In order to correlate the water drop impact damage with material properties an effort was made to obtain samples of materials for which one property was changed while the other properties of the base material remained unchanged: for example, grain size variations, fracture toughness levels, or modified processing procedures. This idealized variation of material properties is rarely achieved. The author gratefully acknowledges the materials received from the individuals listed below for this purpose.

Al_2O_3 - ZrO_2 composites

Courtesy of Dr. Paul F. Becher
Oak Ridge National Laboratory

Pyroceram 9606

Courtesy of Mr. William T. Cahill
Corning Glass Works

Chemically Vapor Deposited (CVD)

Courtesy of Mr. Richard L. Gentilman
Raytheon Company

Hot-Pressed (HP) Magnesium Fluoride
(IRTRAN 1)
HP Magnesium Oxide
(IRTRAN 5)

Courtesy of Mr. Milton S. Gross
Eastman Kodak Company

Al ₂ O ₃ (as-received and annealed)	Courtesy of Dr. Bernard J. Hockey National Bureau of Standards Gaithersburg, MD
Al ₂ O ₃ -ZrO ₂ composites	Courtesy of Dr. F. F. Lange Rockwell Science Center Thousand Oaks, CA
HP Spinel (MgAl ₂ O ₄)	Courtesy of Mr. C. F. Markarian Naval Weapons Center China Lake, CA
HP Spinel (MgAl ₂ O ₄)	Courtesy of Mr. Donald W. Roy Coors Porcelain Company
Silica Mullite (3Al ₂ O ₃ .2SiO ₂)	Courtesy of Dr. Richard A. Tanzilli General Electric Company Re-entry Systems Division
Germania Mullite (3Al ₂ O ₃ .2GeO ₂)	
Yttria-Zirconia Solid Solution (2w/o Y ₂ O ₃)	
Z-6 (100% Tetragonal)	
Z-13 (~49% Tetragonal)	
Z-16 (~45% Tetragonal)	
Z-18 (~55% Tetragonal)	
Aluminum Nitride	
Germanate Glass	

The continued support received from the Office of Naval Research for this work is appreciated.

TABLE OF CONTENTS

<u>SECTION</u>		<u>PAGE</u>
1.0	INTRODUCTION	1
2.0	ADDITIONAL IMPACTS ON ZINC SULFIDE	7
3.0	INFLUENCE OF WATER DROP DISTORTION ON IMPACT DAMAGE .	17
	3.1 BACKGROUND	17
	3.2 EXPERIMENTAL COMPARISONS	18
4.0	INFLUENCE OF MATERIAL PROPERTIES ON WATER DROP IMPACT DAMAGE	25
	4.1 RELATIVE WATER DROP IMPACT RESISTANCE	25
	4.2 MATERIAL PROPERTY CORRELATIONS	27
	4.3 SPECIMEN PREPARATION PROCEDURES	35
	4.4 TEST CONDITIONS	35
	4.5 RESULTS	36
	4.5.1 Fracture Threshold Evaluations	39
	4.5.2 Higher Strength Ceramics	42
	4.5.3 Glasses	52
5.0	EXAMINATION OF WATER DROP IMPACT DAMAGED MATERIALS . .	63
	5.1 MAGNESIUM OXIDE	63
	5.2 SPINEL	69
	5.3 ALUMINA AND ALUMINA/ZIRCONIA COMPOSITES	74
6.0	NYLON BEAD SIMULATION OF WATER DROP IMPACTS	77
7.0	DISCUSSION AND CONCLUSIONS	85
	REFERENCES	90
	TECHNICAL REPORTS FOR CONTRACT NO. N00014-76-C-0744 .	94
	PUBLICATIONS FROM CONTRACT NO. N00014-76-C-0744 . . .	95

LIST OF ILLUSTRATIONS

<u>FIGURE</u>		<u>PAGE</u>
2.1	Impact Damage on Zinc Sulfide Due to a 2.30 mm Water Drop Impacting at 540 ms^{-1}	8
2.2	Cross-Section of Water Drop Impact Damage in Zinc Sulfide Showing Morphology of Dominant Subsurface Fractures	9
2.3	Radial Distance to Dominant Type I and Type II Fractures as a Function of Impact Velocity for Water Drop Impacts on CVD ZnS	12
2.4	Penetration Depth for Type I Fractures as a Function of Impact Velocity for Water Drop Impacts on CVD ZnS	13
2.5	Penetration Depth for Type II Fractures as a Function of Impact Velocity for Water Drop Impacts on CVD ZnS	14
3.1	Influence of Drop Distortion on the Impact Damage Produced in Polymethylmethacrylate	20
3.2	Effects of Drop Diameter and Drop Distortion on the Impact Damage in Zinc Sulfide	22
4.1	Comparison of Extent of Water Drop Impact Damage on Zinc Chalcogenides for Impact Velocities Slightly Above Fracture Threshold Levels	41
4.2	Radial Distance to Dominant Type I and Type II Fractures as a Function of Impact Velocity for Water Drop Impacts on CVD ZnSe and HP ZnS Compared with CVD ZnS Data	44
4.3	Penetration Depth for Type I Fractures as a Function of Impact Velocity for Water Drop Impacts on CVD ZnSe and HP ZnS Compared with CVD ZnS Data	45
4.4	Penetration Depth for Type II Fractures as a Function of Impact Velocity for Water Drop Impacts on CVD ZnSe and HP ZnS Compared with CVD ZnS Data	46
4.5	Subsurface Fracture Pattern for CVD ZnSe	47
4.6	Comparison of Water Drop Impact Damage on Aluminum Nitride, Silica Mullite, and Germania Mullite	49
4.7	Water Drop Impact Damage on Spinel and Pyroceram	50
4.8	Higher Velocity Water Drop Impacts on Unfortified and Fortified Pyroceram	51
4.9	2.25 mm Water Drop Impact on Fused Silica at 361 ms^{-1}	53

LIST OF ILLUSTRATIONS (continued)

<u>FIGURE</u>		<u>PAGE</u>
4.10	2.31 mm Water Drop Impact on Borosilicate Glass at 375 ms ⁻¹	54
4.11	Comparison of Water Drop Impact Damage on Germanate Glass and Magnesium Fluoride	55
4.12	2.31 mm Water Drop Impact on Borosilicate Glass at 469 ms ⁻¹	57
4.13	2.25 mm Water Impact on Soda Lime Glass at 462 ms ⁻¹ . . .	58
4.14	2.30 mm Water Drop Impact on Germanate Glass at 531 ms ⁻¹ .	59
4.15	2.32 mm Water Drop Impact on Magnesium Fluoride at 578 ms ⁻¹	60
5.1	Subsurface Fracture Pattern for a 2.04 mm Water Drop Impact on HP MgO at 715 ms ⁻¹	65
5.2	Overetched Impact Damage Site on CVD MgO for a 2.30 mm Water Drop Impacting at 660 ms ⁻¹	67
5.3	Details of Damage on CVD MgO for the Water Drop Impact Shown in Figure 5.2	68
5.4	Detail of Grain Boundary Features for Spinel with 2 w/o Lithium Fluoride	70
5.5	Influence of Lithium Fluoride Content in Spinel on Water Drop Impact Damage	72
5.6	Comparison of Water Drop Impact Damage on Spinel Samples .	73
6.1	Radial Distance to Dominant Type I and Type II Fractures as a Function of Impact Velocity for Nylon Bead Impacts on CVD ZnS Compared with Water Drop Impact Data	81
6.2	Penetration Depth for Type I Fractures as a Function of Impact Velocity for Nylon Bead Impacts on CVD ZnS Compared with Water Drop Impact Data	82
6.3	Penetration Depth for Type II Fractures as a Function of Impact Velocity for Nylon Bead Impacts on CVD ZnS Compared with Water Drop Impact Data	83

LIST OF TABLES

<u>TABLE</u>		<u>PAGE</u>
2.1	Water Drop Impact Conditions and Subsurface Fracture Measurements for CVD ZnS	11
3.1	Water Drop Impact Conditions and Subsurface Fracture Measurements for Spherical and Distorted Drop Impacts on Zinc Sulfide	21
4.1	Summary of Material Properties	28
4.2	Summary of Fracture Toughness Evaluations for Zinc Sulfide, Zinc Selenide, and Spinel	32
4.3	Water Drop Impact Conditions for Higher Strength Ceramics	37
4.4	Water Drop Impact Conditions for Selected Glasses . . .	38
4.5	Water Drop Impact Conditions and Subsurface Fracture Measurements for CVD ZnSe and HP ZnS	43
5.1	Alumina and Alumina Composites	75
6.1	Fracture Measurements for Nylon Bead Impacts on CVD ZnS	80

1.0 INTRODUCTION

The overall objectives of this program were to generate data which define the rain erosion behavior of ceramic infrared-transmitting window and radome materials and to establish phenomenological and experimental analyses which describe the mechanisms and modes of degradation of material properties. The information obtained will be useful in identifying suitable hardening techniques for future material requirements.

A ballistic range test facility was selected as the most desirable means for obtaining single water drop impacts on brittle and semi-brittle materials, however a number of technical difficulties were encountered in providing the damaged specimens required in this research effort. A significant developmental effort was required to establish suitable stopping and retrieval conditions for the brittle specimens fired down the range which would not introduce any damage other than that due to impact with a single water drop and to eliminate a variety of problems associated with maintaining the integrity of the water drop before impacting the specimen. A completely satisfactory system is now operational.

The Effects Technology, Inc. (ETI) liquid drop impact facility (Adler and James, 1979; Adler, Botke and James, 1979) is unique with regard to the production and characterization of spherical water drop impacts over an extended velocity range (currently 150 to over 1000 ms^{-1}). Due to the inherent complexity of the erosive response of materials in a multiple water drop environment, this investigation concentrated on a very idealized water drop impact condition: the normal collision of a spherical water drop with a plane surface. However, drop distortions can be introduced in a controlled manner for simulating more representative aerodynamic conditions.

During the course of this investigation the limits on the range of impact velocities in the ballistic range facility have increased from the required 400 ms^{-1} at the initiation of this program to over 1000 ms^{-1} and decreased to approximately 150 ms^{-1} . The upper velocity was achieved by redesigning the sabot containing the specimen and the protection provided

the specimen when it was inserted in the sabot. The lower velocity regime (150 to 250 ms⁻¹) is required to determine the fracture threshold for water drop impacts in low to moderate hardness materials such as zinc sulfide and zinc selenide. These velocities presented a problem because the velocity is controlled by the manner in which a very small quantity of gunpowder burns in the breech of the gun barrel. The velocity is extremely sensitive to small changes in the burn rate. A moderate developmental effort was required to achieve satisfactory control on the velocity so that the drop could be photographed prior to impact.

The sphericity of the drop just prior to impact was confirmed in a small test series. This was made possible through the acquisition of a nanosecond flash unit which provided excellent definition of the periphery of the drop than was previously available.

The perfection of the water drop impact damage generated in the ETI liquid drop impact facility has been used as a basis for comparison with the damage produced in rotating arm erosion facilities, in ballistic ranges, by water jet simulations of water drop collisions, and by nylon bead simulations of water drop collisions. Published comparisons (Adler, 1979c; Adler, Botke and James, 1979; Adler and James, 1980) have alerted the rain-erosion community to the potential errors which may exist between the impact conditions actually occurring and those simply assumed to be taking place. This investigation has shown that drop distortion prior to impact is very difficult to eliminate in experimental facilities and that moderate levels of drop distortion cannot be detected from post-test examination of the surface fractures in brittle ceramics.

In addition to accurately characterizing the water drop impact conditions for modeling studies, alternative procedures have been considered for simulating the effects of water drop collisions. Two water drop simulations were investigated: water jets and nylon beads (or soft body) collisions (Adler and James, 1980). Both simulations offer flexibility in the specimen geometry since the impacting mass is propelled against a stationary target. This affords an opportunity to investigate impacts on

fabricated optical components, to conduct tests at elevated temperatures, and to provide test specimens for residual strength measurements. The nylon bead collisions can be used to gain understanding of water drop impacts from 1000 to above 4000 ms⁻¹ (using ETI's capacitor-discharge, particle acceleration facilities). Five different nylon formulations were considered for ease of producing spherical beads and similarities in the damage produced compared with water drop impacts. One nylon formulation was found to satisfy these requirements. The resulting nylon bead impact damage is close enough to that produced by water drops to be a viable alternative. On the other hand water jet impacts which are supposed to simulate water drop collisions for reasonable drop sizes (on the order of 1 mm) require extremely small orifice diameters beyond 600 ms⁻¹, so from a pragmatic viewpoint the water jet may not be appropriate for such drops impacting at velocities above 600 ms⁻¹ (J.E. Field, et al. 1979). In addition the impacts examined from the lower velocity impacts indicate that subsurface fractures produced by nylon bead impacts are nearly identical to the subsurface fracture patterns for water drop collisions, whereas the water jet impacts display a distinctly different form of subsurface fracture response (Adler and James, 1980).

A reproducible, controlled, and well-characterized impact condition is necessary if an accurate assessment of a material's deformation and fracture response is to be established for water drop impact loadings. These conditions are quite desirable for analytical and finite difference evaluations of the impact process. Moderately detailed microscope examinations of several water drop-impacted materials (polymethylmethacrylate, magnesium oxide, calcium fluoride, and polycrystalline zinc sulfide) have been completed to provide a reasonably comprehensive picture of the deformation and fracture response for these materials which was somewhat confused in previous publications (Lankford and Leverance, 1971; Lankford, et al. 1973; Behrendt, 1974; Jolliffe, 1966; Hoagland and Jung, 1978). In particular, spherical water drop-induced fractures in CVD zinc sulfide have been investigated in considerable depth (Adler and James, 1980). Measurements of the identifiable features of the impact damage have been made which provide a data base for this material at impact velocities from 200 to 800 ms⁻¹. This data has been used to investigate the existing

analytical concepts of the loading conditions for water drop collisions and the nature of the transient stresses generated in the target material which promote fracture. Excellent agreement was found between the experimental measurements and the analytical results due to the well-characterized experimental conditions.

During the period that the single water drop impact facility was being developed, the loading characteristics due to solid particle impingement on material surfaces were analyzed, both high and low velocity solid particle impacts on single crystals were carried out, and multiple water drop impacts at subsonic velocities were investigated (Adler and Hooker, 1977; Hooker and Adler, 1978).

Analytical studies demonstrated that at impact velocities below 1000 ms^{-1} :

- The magnitude of the contact pressure, the radius of the contact zone, and the rate of expansion of the contact zone for a water drop cannot all be approximated by a hard solid particle.
- The magnitude of the contact pressure is considerably larger (ranging from 5 to 20 times) for hard solid particles compared to water drops.
- The contact zone for water expands at a rate roughly two orders of magnitude faster than an equivalent solid particle.
- The differences between nylon bead and water drop impacts are considerably less than hard solid particles, however
 - nylon is assumed to load the surface at a slower rate and produce higher shear forces on the surface than water;
 - at low impact velocities nylon has the capacity to rebound from the surface whereas water does not.

A description of the response of several materials to solid particle impacts can be found in the report by Adler and Hooker (1977).

At the present time, a number of developmental materials for advanced systems are becoming available in a form suitable for material property evaluations. Effects Technology, Inc., is in a unique position for providing a reliable assessment of the rain erosion resistance for the full range of hardened radome and infrared-transmitting material candidates. Several examples of water drop impact damage in both commercially-available and developmental materials are provided in this report as well as our previous work (Adler and James, 1979, 1980).

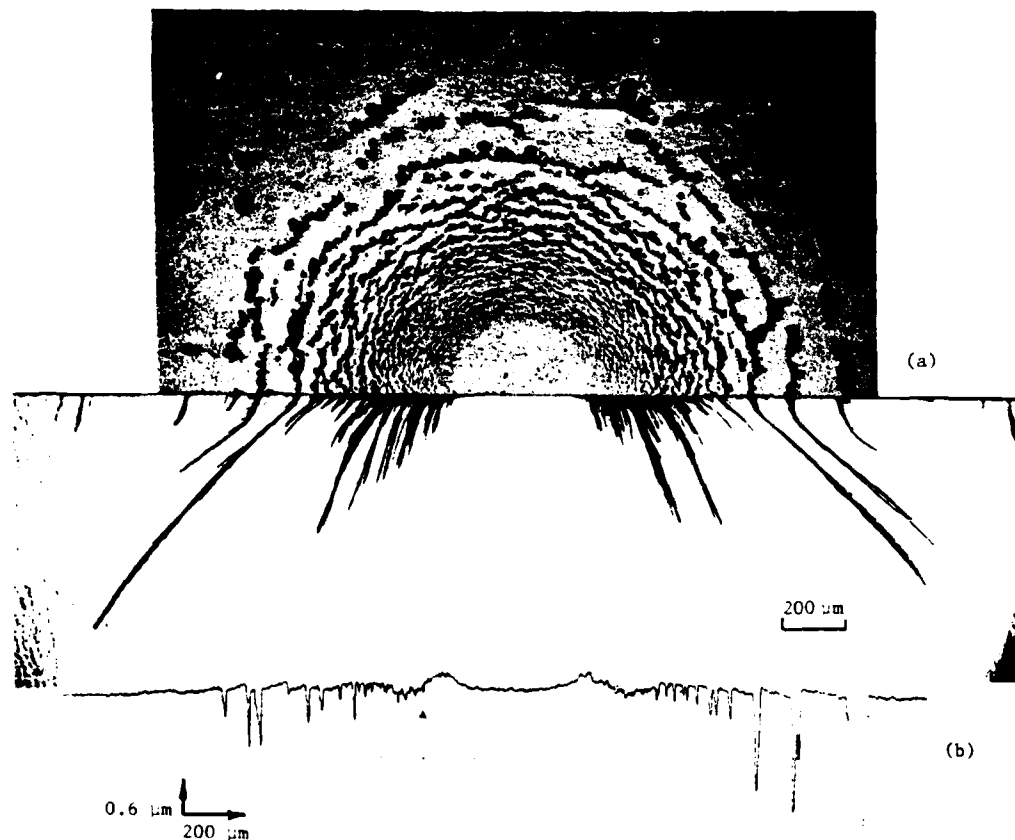
The purpose for developing the experimental capability was to investigate the response of ceramic materials due to a definable and reproducible water drop impact loading condition. This experimental capability, which did not exist in the field of rain erosion, has been instrumental in constructing accurate concepts of the water drop/target interactions and providing a physical basis for the development of meaningful correlations between the observed water drop impact damage and the material properties of the target materials. Impact damage characterization procedures have also been developed and are fairly well established in our laboratory for a variety of ceramic materials.

2.0 ADDITIONAL IMPACTS ON ZINC SULFIDE

The general character of the fractures produced by water drop collisions in zinc sulfide have been described by Adler and James (1980). The main observation from this work was the presence of two distinct types of fractures: referred to as Type I and Type II fractures. An overview of the impact damage is provided in Fig. 2.1. As seen in cross-section, the Type I fractures in the region adjacent to the central undamaged zone approach the surface at shallow angles. The Type II fractures occur at larger radial distances. The Type II fractures approach the impact face at very steep angles and often display a reversed curvature. In order to quantify the extent of the damage for a particular impact condition, measurements are made of the location, depth and approximate orientation of the dominant Type I and Type II fractures. This idealization of the subsurface impact damage is illustrated in Fig. 2.2. Two forms of Type II fractures are observed; they will be described later.

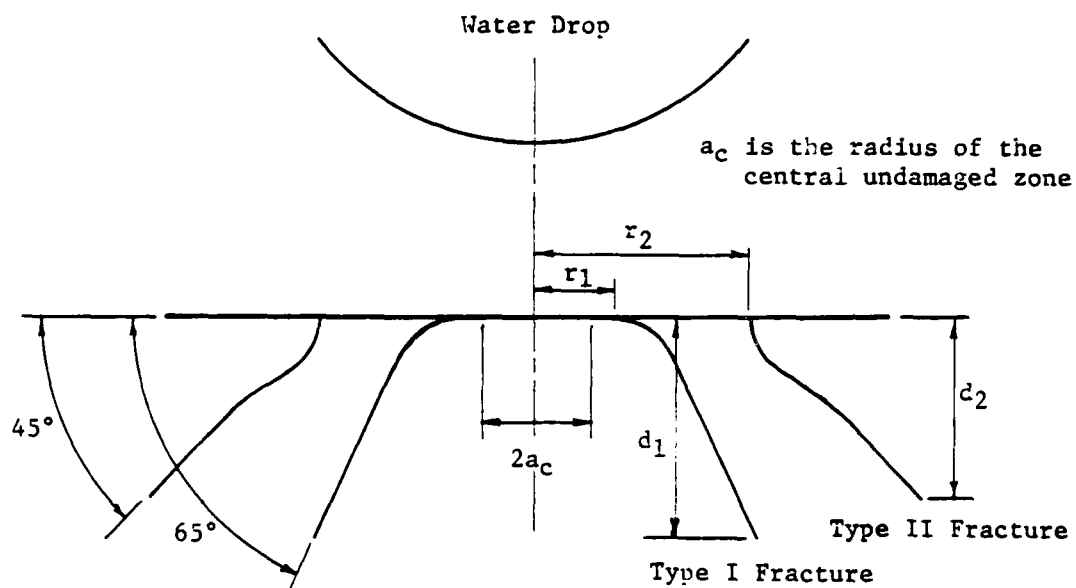
The radial location of the dominant Type II fracture exhibits a high degree of variability as can be seen from the previous measurements (Adler and James, 1980). The radial locations of the dominant Type I fractures are considerably better defined. The actual fracture patterns present a distribution of fractures and the idealized configuration (Fig. 2.2) is not always achieved. Additional water drop collisions were obtained in CVD ZnS in order to investigate the significant increase in the radial location of the Type II fracture found previously (Adler and James, 1980) when the impact velocity exceeded 500 ms^{-1} .

A single thin section is obtained from each impacted specimen. A diameter through the impact site is selected as being representative of the average damage when viewed microscopically using transmitted light illumination. The diameter is chosen based on the perfection of the fractures along this line, that is, there are no unusual features due to imperfections in the water drop and there are no significant surface scratch initiated fractures. The later occurrence results in fracture depths which are much greater than the fractures produced by relatively small surface flaws. The specimen is mounted in an epoxy resin and is sectioned slightly away from the diameter selected. The cross-section is then polished and the polished

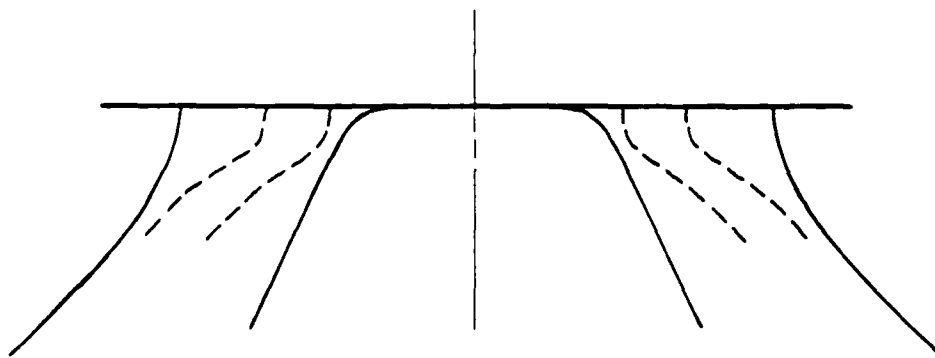


- (a) Circumferential fractures seen in reflected light illumination with subsurface fractures on thin section through center of impact. Note the increasing level of radial outflow damage with distance from the center of impact.
- (b) Surface profile along center line of impact damage.

Figure 2.1. Impact Damage on Zinc Sulfide Due to a 2.30 mm Water Drop Impacting at 540 ms^{-1} .



a. Idealized Subsurface Fracture Pattern



b. Alternative Forms of Subsurface Fracture Pattern. Double Recurve Type II Fracture Displays Significant Variability in Location. Single Convex Fracture Often Is Identified as Dominant Type II Fracture.

Figure 2.2. Cross-Section of Water Drop Impact Damage in Zinc Sulfide Showing Morphology of Dominant Subsurface Fractures.

face is bonded to a glass plate. The remaining portion of the specimen is removed by cutting parallel to the initially exposed face at a distance of approximately 1 mm. This face is then polished for viewing the subsurface fractures. The cross-section is photographed using transmitted light and the various measurements are made directly from the negative. This is accomplished by projecting the image onto a white surface using a photographic enlarger. A 0.01 mm scale is also photographed and projected to obtain the magnification factor for converting the measurements to their actual values. The measurements made in this way are summarized in Table 2.1 and plotted on the original data from Adler and James (1980) in Fig. 2.3 to 2.5.

Obviously this procedure is quite subjective and can only provide an approximation to the average fracture location and depth, since the discrete fractures are circumferential segments located at different radial distances from the center of impact and with significant variations in the maximum depth within an annulus surrounding the impact site. However this procedure is useful as an initial means for evaluating the impact damage. Improvements in the sectioning procedure have made it possible to observe more details of the fractures in the vicinity of the impacted surface.

With the introduction of additional measurements the general trend in the velocity dependence of the radial distances in Fig. 2.3 exhibits a slightly different form than previously reported by Adler and James (1980). The velocity dependence of the fracture depths does not show any significant differences from the previous trends.

The identification of the dominant Type II fracture is quite difficult. The maximum fracture depth in this region is often used to find the dominant fracture. A double recurve fracture trajectory is often seen nearly adjacent to the dominant Type I fracture or a single curved trajectory is dominant at much larger radial distances (as illustrated in Fig. 2.2). An effort was made to sort the cross-sections into categories for which either of these two forms of fractures were dominant, however no correlation with the impact conditions could be established.

The identification of the subsurface fractures and their measurement has been useful in understanding and quantifying the effects of the water

Table 2.1. Water Drop Impact Conditions and Subsurface Fracture Measurements for CVD ZnS

Shot No.	Impact Velocity (ms ⁻¹)	Drop Diameter (mm)	2a _c (mm)	Type I Fractures		Type II Fractures	
				Location (mm)	Depth (mm)	Location (mm)	Depth (mm)
1319	494	2.04	0.38	0.42	0.58	0.79	0.47
1296	512	2.19	.40	.39	.42	.78	.33
1302	552	2.19	.38	.47	.59	.85	.66
1317	600	2.12	.39	.43	.55	.98	.70
1437	487	2.28	0.20	0.44	0.43	0.70	0.55
1445	524	2.25	.30	.46	.47	.75	.70
1431	552	2.28	.38	.41	.48	.76	.75
1430	555	2.23	.39	.43	.55	.96	.62
1433	595	2.23	.41	.48	.72	.98	.77
1436	621	2.20	.40	.50	.94	1.17	.93
1447	621	2.28	.35	.58	.86	1.24	.80
1435	644	2.25	.44	.56	.92	1.28	.87

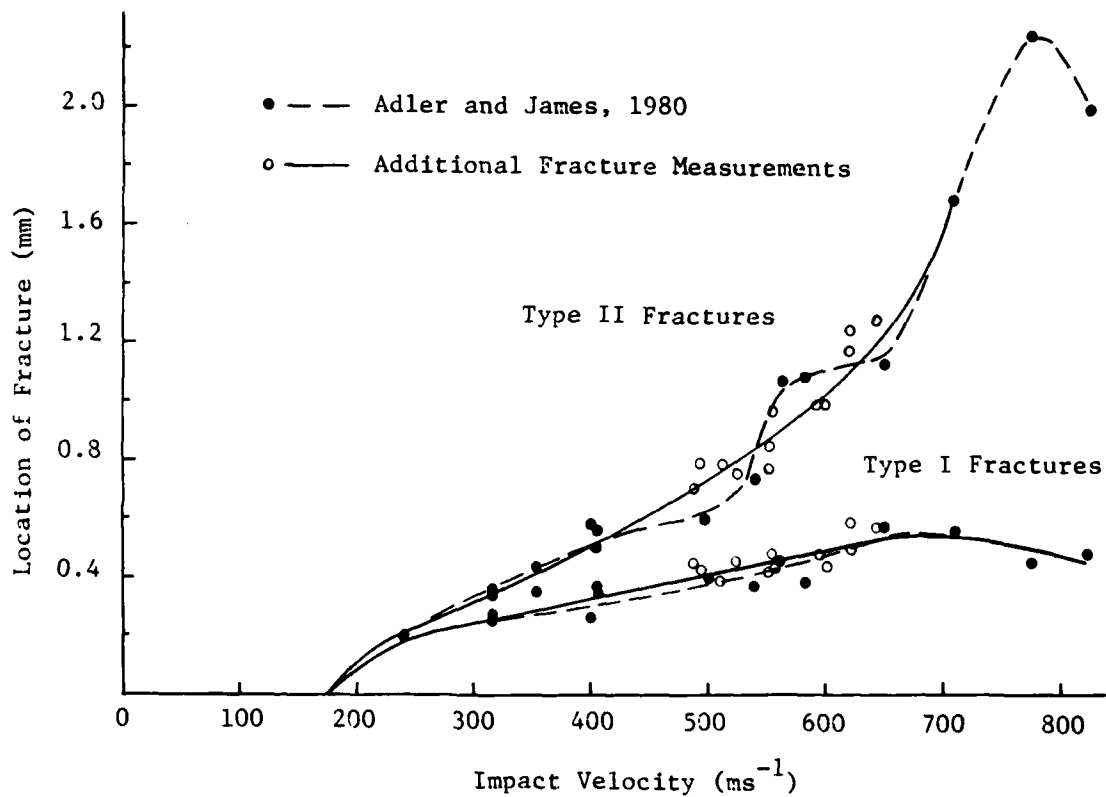


Figure 2.3. Radial Distance to Dominant Type I and Type II Fractures as a Function of Impact Velocity for Water Drop Impacts on CVD ZnS.

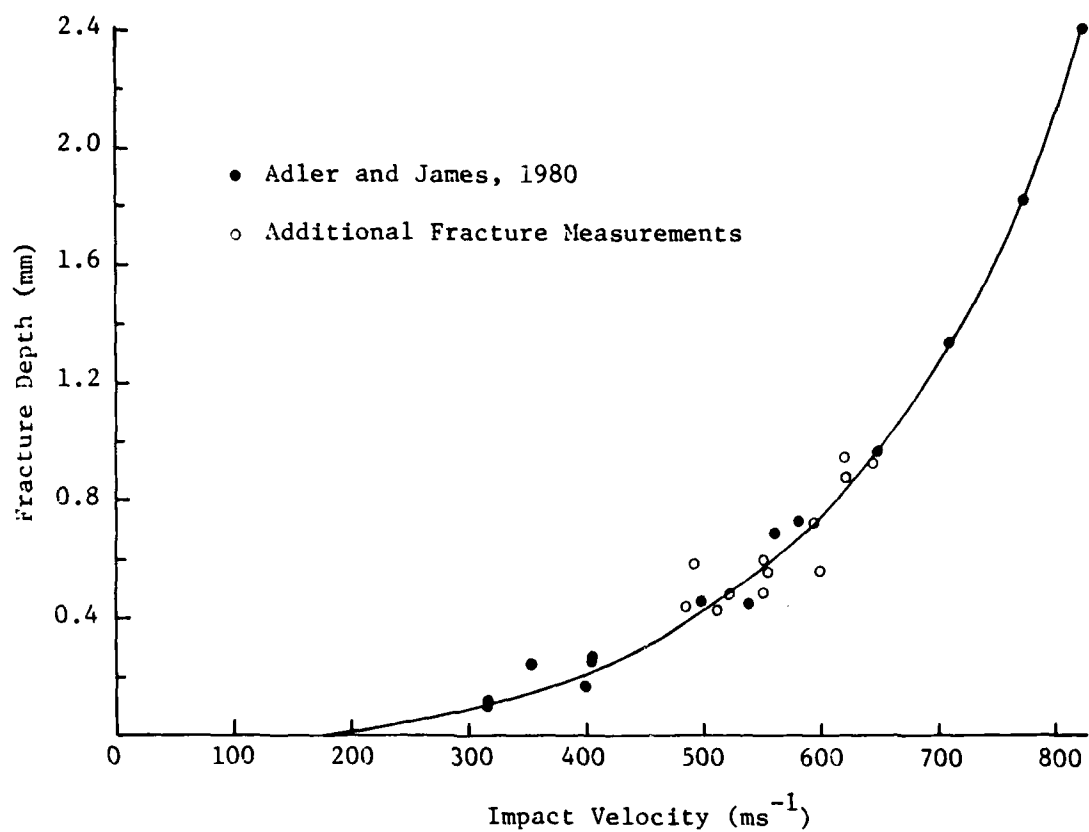


Figure 2.4. Penetration Depth for Type I Fractures as a Function of Impact Velocity for Water Drop Impacts on CVD ZnS.

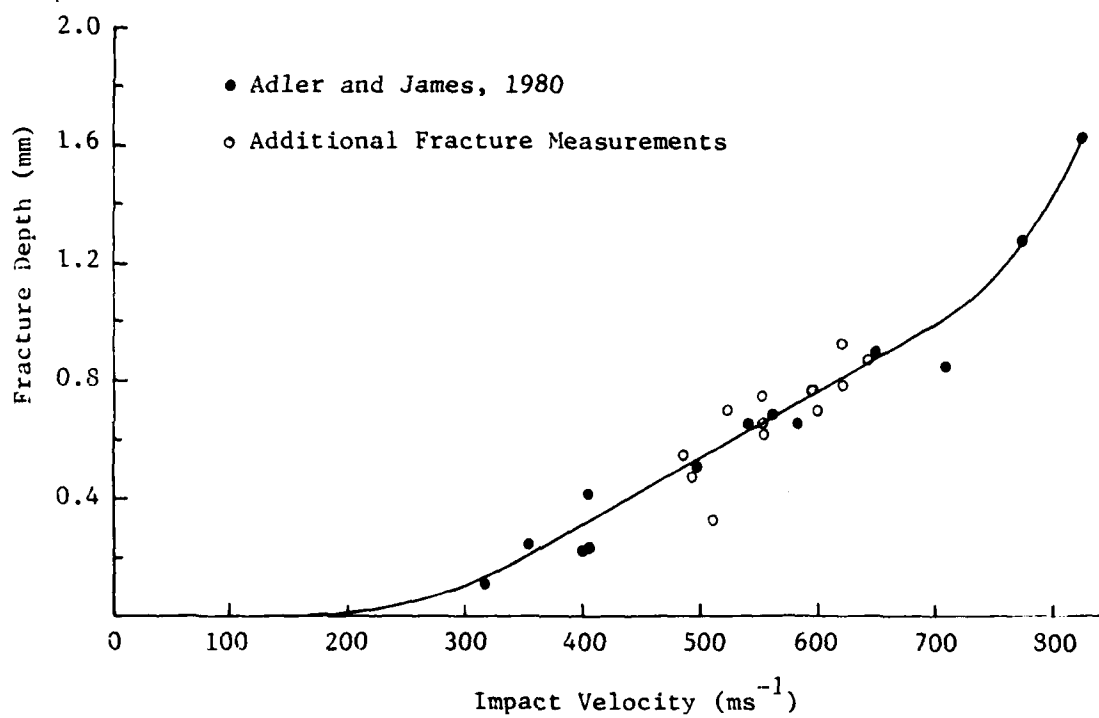


Figure 2.5. Penetration Depth for Type II Fractures as a Function of Impact Velocity for Water Drop Impacts on CVD ZnS.

drop collisions in materials for which mass removal is not a meaningful measurement. The fracture measurements are essential for estimating the transmission losses and residual strength of infrared-transmitting windows. The development and implementation of more refined measurement procedures would certainly be helpful in expanding the fracture data base.

3.0 INFLUENCE OF WATER DROP DISTORTION ON IMPACT DAMAGE

The condition of a water drop prior to impacting a vehicle in flight has a strong influence on the extent of the damage which results from this collision. The significance of this statement cannot be overemphasized since this is the critical element, so often not appreciated, which is responsible for the differences observed in the results obtained from various water drop impact facilities: rotating arms, ballistic ranges, and rocket sleds. The water drops are usually assumed to be spherical and of a uniform size. Generally there is no confirmation that this is actually the case in a particular facility. Therefore, on the basis of our current understanding of water drop impact damage, a significant level of uncertainty exists for results obtained from a facility for which direct observation of the water drops are not made just prior to colliding with the target's surface. A study was undertaken which illustrates the significance of drop distortion on the level of damage generated by the collision using well-characterized experimental conditions. The ETI liquid drop impact facility was used for this purpose.

3.1 BACKGROUND

Relatively little work has been done on quantitatively evaluating the influence of drop distortion on the extent of water drop impact damage. However, this information is essential for utilizing laboratory data for predicting in-flight erosion damage. The general procedure for making physically reasonable predictions of rain erosion damage has been outlined by Adler (1979a, 1981). Recognizing that all of the possible in-flight conditions cannot be reproduced in ground test facilities, the test results must be used in conjunction with analyses of the flow fields around the vehicle during its flight trajectory. The boundary layer thicknesses and shock fronts are computed for the actual flight conditions. Correlations of the degree of drop distortion in aerodynamic flow fields, such as those provided by Ranger and Nicholls (1969) and Waldman, et al. (1972), can then be used to determine the level of distortion the drop will experience prior to striking the surface of the vehicle. Thus once a suitable laboratory data base is available for defining the damage produced in a candidate material for a range of drop dimensions, drop distortion levels, impact velocities, impact angles, and

multiple water drop interactions, accurate predictions of the rain erosion effects can be made for essentially arbitrary flight scenarios.

Obviously establishment of the water drop impact damage data base for the indicated range of impact parameters would involve extensive testing and damage characterization. The scope of such an undertaking may therefore be impractical, although the total cost involved in providing a useful test matrix is estimated to be less than generating data in an elaborate test facility with little control and evaluation of the water drop impact conditions. In these terms the suggested approach has considerable merit. Alternatively the water drop impact test matrix can be scaled to a level which would at least provide general trends in the material response as a function of the relevant impact parameters. Reasonable estimates could conceivably be obtained of the rain erosion effects on this basis.

3.2 EXPERIMENTAL COMPARISONS

Water drops with diameters of approximately 1.8 and 3.2 mm were used to impact CVD ZnS targets in order to determine the damage produced by both spherical and ellipsoidal-shaped drops. The 3.2 mm water drop represents a six-fold increase in the amount of water impacting the target.

These experiments were carried out in the ETI water drop impact facility which provides highly-controlled and well-documented water drop impact conditions (Adler and James, 1979; Adler, Botke and James, 1979). Spherical water drops are produced for impact velocities ranging from 200 to 1000 ms^{-1} . Approximate ellipsoidal-shaped drops are generated by increasing the ambient pressure in the system which is usually purged with helium in order to minimize the aerodynamic effects on the falling water drop. By varying the ambient pressure, so that the amount of helium remaining in the gun barrel is compressed ahead of the specimen as it travels down the barrel, any desired level of drop distortion can be achieved including stripping and shattering of the drop. The ratio of the major to minor axis in this test series was varied from 1.0 to 1.5 so the level of distortion was not extreme.

Many examples of the distorted drops can be shown, however the 2.2 mm water drop impacts on polymethylmethacrylate in Fig. 3.1 provides a general overview of the experimental conditions and the extent of the damage produced. The impact velocity for both the spherical and distorted drops is 495 ms^{-1} . The ratio of the major to minor axis of the distorted drop is 1.19. The diameter of the impact damage site for the distorted drop shows a significant increase over that for the equivalent spherical drop.

The comparison points out that without direct observation of the water drop just prior to impact there would be no indication that the drop was distorted based solely on post-test examination of the impact damage. This may be one of the reasons why the erosion data from facilities with essentially equivalent impact conditions does not show more consistent agreement.

Measurements of the Type I and Type II fractures, described in Section 2, are provided in order to quantify the extent of the damage which may be generated by increased drop diameter, impact velocity, and drop distortion. The measurements for these fracture parameters for the various impact conditions are listed in Table 3.1. The fracture parameters, due to a distorted water drop, are compared with the same measurements for the damage produced by an equivalent spherical water drop. The general features of the impact sites and some idea of the relative changes in the extent of the damage due to drop diameter and drop distortion can be seen in Fig. 3.2.

Referring to Table 3.1, a significant difference is noted in the fracture measurements for Shot No. 1511 and 1513 which represent about the same impact condition. The thin section for Shot No. 1517 was destroyed during final preparation so no fracture measurements were obtained for this impact condition. The drop for Shot No. 1518 was to be a 3.2 mm drop as determined by its equivalent mass, but instead an inordinately large drop was generated during this test. The sizable difference in drop diameter, 3.55 mm as opposed to 3.2 mm, was a rare occurrence, since the variation of drop diameters from test to test is typically no more than 5 percent.

An effort was made to rectify the inconsistent data. Excellent additional water drop impacts were obtained in all cases, but unfortunately the



a. 2.18 mm Spherical Water Drop Impacting at 495 ms^{-1} .

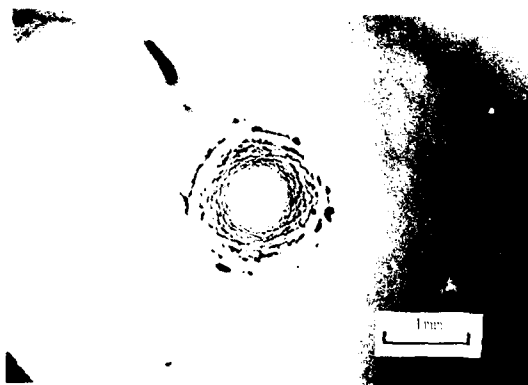


b. Distorted Water Drop Impacting at 495 ms^{-1} (Aspect Ratio 1.19).

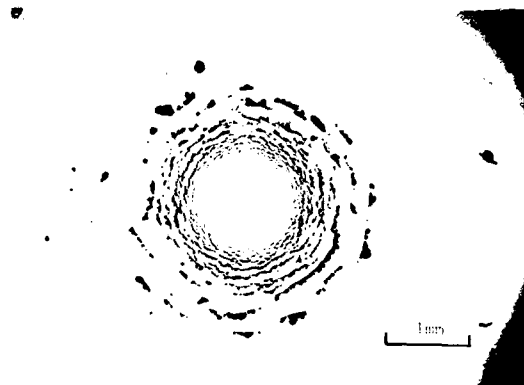
Figure 3.1. Influence of Drop Distortion on the Impact Damage Produced in Polymethylmethacrylate.

Table 3.1. Water Drop Impact Conditions and Subsurface Fracture Measurements for Zinc Sulfide.

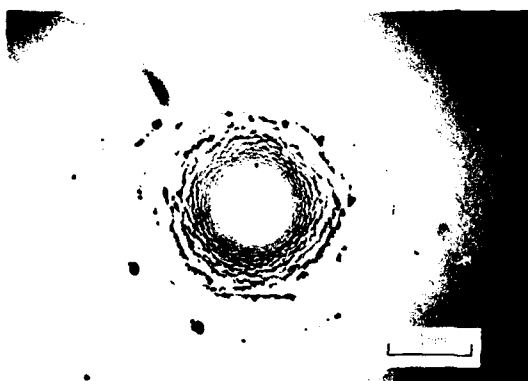
Shot No.	Impact Velocity (ms ⁻¹)	Drop Major Axis (mm)	Drop Minor Axis (mm)	Aspect Ratio	Volume (mm ³)	Equivalent Spherical Drop Diameter		2a _c (mm)	Type I Fractures		Type II Fractures	
						Based on Mass (mm)	Based on Radius of Curvature (mm)		Location (mm)	Depth (mm)	Location (mm)	Depth (mm)
1508	378	1.82	1.77	1.03	3.05	1.80	-	0.30	0.215	0.11	0.325	0.125
1522	375	2.07	1.40	1.48	3.14	1.82	2.84	.36	.385	.195	.605	.235
1519	373	3.26	3.26	1.00	18.14	3.26	-	.48	.56	.555	1.065	.47
1515	384	3.38	2.92	1.16	17.47	3.22	4.33	.45	.625	.615	1.085	.675
1510	542	1.79	1.73	1.03	2.85	1.77	-	.32	.385	.335	.805	.235
1511	505	2.02	1.44	1.40	3.08	1.80	2.69	.50	.53	.265	.765	.405
1513	532	2.02	1.44	1.40	3.08	1.80	2.69	.50	.45	.625	.97	.67
1517	494	3.19	3.07	1.04	16.06	3.15	-	Section damaged in preparation				
1518	513	3.65	3.36	1.09	23.44	3.55	4.27	.60	.74	1.25	2.19	1.225



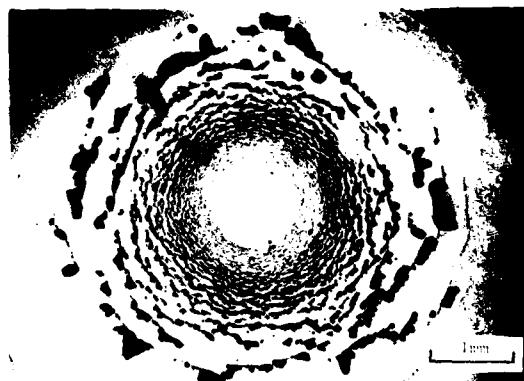
a. Shot No. 1510:



b. Shot No. 1517:



c. Shot No. 1511:



d. Shot No. 1518:

Figure 3.2. Effects of Drop Diameter and Drop Distortion on the Impact Damage in Zinc Sulfide

surface finish on the specimens used in this test series was unacceptable. It was not possible to define cross-sections which would not be influenced by surface scratch interactions.

The curvature of the front face of the distorted drop was used to determine the diameter of an equivalent spherical drop with this curvature. An alternative procedure for establishing the equivalent spherical drop would be in terms of the mass of water in the distorted drop. Both of these measurements are recorded in Table 3.1. According to the predictions from the mechanics of a water drop collision, the damage produced should be primarily dependent on the curvature of the front face of the drop, as long as the drop distortion is not extreme, and to a lesser extent on the mass of liquid impacting the surface (Adler, 1979b; Adler, Botke, and James, 1979).

Although precise identification of Type I and Type II fractures is not always evident and the circumferential variation of these measurements is fairly great, the general trend in the data is clear. A slightly distorted drop is significantly more damaging than a spherical drop. The magnitude of these differences can be approximated from the measurements recorded in Table 3.1. The measurements in Table 3.1 for spherical 1.8 mm diameter drops are consistent with the general trends for 2.2 mm spherical water drop impacts reported in Section 2.

The fracture depths for both the Type I and Type II fractures for 1.8 mm drops impacting at 375 ms^{-1} and 540 ms^{-1} show a significant (almost two-fold) increase for a distorted drop compared with a spherical drop, i.e., comparing Shot No. 1522 to 1508 and Shot No. 1513 to 1510 in Table 3.1. The effect of the increase in velocity is evident by comparing Shot No. 1508 with 1510. The ratio of the increase in Type I fracture depths with velocity is essentially identical for the 1.8 mm drops used here and the 2.2 mm drops used previously. The ratio of the increase in Type II fracture depths for the same two impact conditions is not as consistent.

It is concluded, based on the results from well-controlled water drop impact experiments, that slightly distorted drops can be significantly more damaging than spherical drops. However suitably defined experimental

conditions can be used to provide a quantitative measure of the rain erosion damage which may take place in a flight environment.

Since only a limited number of distorted drop collisions were investigated and the data for spherical drops with varying diameters is incomplete, it is not possible to determine at this time if the fracture measurements are representative of the damage due to an equivalent spherical drop whose diameter is evaluated on the basis of mass or the front face radius of curvature. This issue deserves further attention.

4.0 INFLUENCE OF MATERIAL PROPERTIES ON WATER DROP IMPACT DAMAGE

Increased hardness, fracture toughness, and elastic wave velocities have been suggested as properties which control the onset and extent of fracture due to particle collisions on ceramic materials. However, the experimental results for water drop impacts indicate that the existing material property correlations do not properly rank the materials on the basis of the observed water drop impact damage. In the case of several glasses with similar material properties, the extent of the damage displays a large variation which cannot be accounted for based on the existing material property correlations. The general conclusion from this work is that the material properties which significantly control water drop impact damage in ceramics have not yet been identified.

The character of the damage produced by multiple water drop impacts is dependent on the magnitude of the impact velocity compared with the fracture threshold for a particular material. The damage mechanism and possibly the controlling material properties will be different depending on whether the intensity of the water drop collision is below or above the fracture threshold. In addition, the intensity of the water drop impact can become so severe (as the impact velocity increases) that a crater will be formed for a single impact. The impact velocities of concern here range from the fracture threshold to less than the level required to produce significant cratering.

4.1 RELATIVE WATER DROP IMPACT RESISTANCE

The typical basis for evaluating a material's erosion resistance is to obtain a measure of the mass removal rate for a standard erosive environment. The steady state mass removal rate is the most meaningful measurement in this regard. However, this parameter is of little concern for infrared-transmitting windows exposed to rain erosion conditions for which the optical transmission degrades to unacceptable levels prior to the onset of any significant mass removal from the exposed surface. In this case there is a need for a more relevant basis for comparison. The optical degradation due to water

drop collisions depends on the impact conditions at which the onset of fracture occurs, the character of the fractures generated once the fracture threshold conditions are exceeded, and the rate of growth of preexisting fractures due to subsequent water drop impacts.

Accurate experimental determinations of the fracture threshold are just beginning to be made. It is quite difficult to experimentally define the onset of fracture which is dependent on how detailed an examination of the impacted surface is conducted, for example, the magnification at which observations are made and what fracture enhancement techniques are introduced. Furthermore, for a high level of refinement it is imperative that the impact condition be precisely determined. In most water drop impact facilities this latter condition cannot be satisfied. The ETI liquid drop impact facility is one of the few facilities that can effectively evaluate the fracture threshold due to spherical water drop impacts (allowing for the statistical nature of the fracture initiation process in polycrystalline ceramics).

Once the fracture threshold velocity has been exceeded there are several types of fractures which can be produced by water drop collisions on fine-grained ceramic materials, however circumferential fracture arrays are generally found at moderate increases in the impact velocity beyond the fracture threshold level. As more experience is acquired in examining the details of these fractures, both at the surface of the target and within the target, distinctive features are beginning to be observed for different materials. The orientation of the internal cracks and separation distance between the crack faces have been identified as influencing the level of transmission resulting from water drop impact damage (Adler, Botke, and James, 1979). The dominant crack orientations can be obtained from cross-sectioned specimens, however the crack separation distances are extremely difficult to determine. It is knowledge of the material dependence of these fracture characteristics which will contribute to improved optical quality in rain erosive environments. At the present time little is known about the factors which contribute to the crack morphology, but headway may be possible through controlled water drop impact experiments on specially fabricated and well-characterized materials.

Another consideration is the crack growth which results when a water drop impacts in the vicinity of a pre-existing crack. Until definitive evidence to the contrary is available, it is hypothesized that subsequent crack growth, both with respect to magnitude and orientation, will be material dependent. Thus, the effectiveness of a material to maintain its optical qualities in an adverse environment cannot be determined solely on the basis of the damage produced by a single water drop impact event. The mission requirements, the flight trajectory, and the environments to be encountered should be used to determine the most detrimental impact conditions for the window material. If the experimentally-determined fracture threshold exceeds these by a safe margin, the damage due to subsequent impacts may not be significant enough to influence the outcome of the mission. If the fracture threshold is below the most detrimental conditions to be encountered, then very complete evaluations of the water drop impact damage are necessary in order to determine if at least a minimum level of window performance is feasible.

From the above discussion it should be realized that a simple procedure for evaluating the rain erosion behavior of ceramic electromagnetic window materials is not yet available. For the purpose of establishing a relative measure of the susceptibility of various materials to water drop impact damage, very superficial microscopic comparisons of the severity of the circumferential fractures for roughly similar impact conditions were used. The reason for the superficial comparisons is that the scope of the program did not allow sectioning and etching procedures to be developed for all of the materials subjected to water drop impacts. A considerable amount of time was devoted to sectioning spinel specimens, however identification of the subsurface fracture trajectories was quite difficult in most cases due to the large grain size (on the order of 60 μm).

4.2 MATERIAL PROPERTY CORRELATIONS

A number of materials have been evaluated in the water drop impact experiments. A selection of these materials is listed in Table 4.1. When available, the relevant material properties are also listed in Table 4.1. The nature of the impact damage produced and whatever material property

Table 4.1. Summary of Material Properties

Material	Specimen Dimensions		ρ (kg/m^3)	E (GPa)	ν	c_l (m/s)	c_s (m/s)	H_k (GPa)	K_c ($\text{MPa m}^{1/2}$)	v_{FT} (m/s)
	Diameter (mm)	Thickness (mm)								
Silica Mullite	18.87	4.24	3170	179	(0.25)	8232	4753	14.2	2.3	214
Germania Mullite	11.15	3.51	3670	138	(0.25)	6717	3878	11.0	2.2	194
Aluminum Nitride	19.05	5.84	3260	317	0.21	10462	6340	12.3	4.2	352
Yttria Zirconia Z6	14.45	3.05	6030	200	(0.25)	6309	3642	9.8	4.0	283
Yttria Zirconia Z13	14.68	2.95	6030	200	(0.25)	6309	3642	9.8	5.0	328
Yttria Zirconia Z16	14.73	3.00	6030	200	(0.25)	6309	3642	9.8	5.0	328
Yttria Zirconia Z18	14.68	3.00	6030	200	(0.25)	6309	3642	9.8+	4.0-5.0	283-328
Pyroceram Corning 9606	15.88	9.53	2600	120	0.245	7408	4305	6.98	1.0-3.0	119-248
Germanate Glass	18.95	c. 6.30	4850	104	0.25	5073	2930	5.53	1.6	162
Soda Lime Glass Corning 0080	19.00	6.00	2470	70	0.22	5688	3430	4.56	0.70	98
Borosilicate Glass Corning 7740	19.00	5.60	2230	64	0.20	5647	3460	4.10	0.716	100
Fused Silica Corning 7940	17.00	9.00	2200	72	0.16	5904	3780	4.80	0.73	105
Magnesium Fluoride IRTRAN 1	20.00	8.00	3130	117	(0.3)	7090	3790	6.0	0.9	124
CVD Zinc Sulfide Raytheon	15.88	8.00	4080	74	0.3	4960	2600	2.5	0.60-1.0	80-113
HP Zinc Sulfide IRTRAN 2	15.88	6.35	4090	97	0.3	5658	3020	2.5-3.54	0.44-0.6	67-84
CVD Zinc Selenide Raytheon	15.88	8.00	5270	67	0.3	4150	2220	1.0	0.68-0.90	83-100
Spinel	17.00	5.00	3630	250	(0.3)	9630	5150	16.0	1.16-2.2	157-240

correlations become evident will be described. In general, the analytical approaches to water drop impact collisions have been concerned with the dynamics of a drop impacting a rigid surface and the transient stresses generated in the target material (Adler, 1979b). The material property correlations that can be found in the rain erosion literature are primarily empirical correlations for metallic and polymeric materials (Adler, 1979b; Brunton and Rochester, 1979). At the present time only Evans, and his co-workers, (Evans, Ito, and Rosenblatt, 1980) have attempted to relate the onset of soft body impact damage in ceramic materials to their properties. The predictions for the fracture threshold impact velocity relation are compared here with results from well-documented water drop impact experiments.

Identification of material properties which influence the particle impact damage in electromagnetic window materials is useful in providing guidance for improving the erosion resistance of developmental materials. On the basis of prior work, increased hardness, fracture toughness, and elastic wave velocities have been suggested as material properties which control the onset and extent of fracture due to particle collisions in ceramic materials (Rosenblatt, et al., 1979; Musikant, et al., 1980). These material properties are tabulated in Table 4.1 for several materials. The material properties for the materials in Table 4.1 were obtained from several sources. The Knoop hardness is also listed in Table 4.1 since it is often assumed that hardness influences the particle impact response of ceramic materials. When a significant range is found in the values in the literature for a particular property, the range of values is recorded in Table 4.1. Wide discrepancies are associated primarily with the fracture toughness evaluations.

It appears that as the number of measurements increases and the test methods used are expanded, the spread in the value of the material property being measured increases. Thus a single value for a particular property should not be interpreted that this value is precisely determined and universally accepted, but rather that only one reliable value could be found in the existing literature. The value reported is therefore subject to change dependent on the fabrication procedures used for different lots of

the same generic material and the material property measurement technique employed. The influence of the test method is amply demonstrated for Pyroceram 9606 where the fabrication procedure is established, but a recent series of round-robin measurements of fracture toughness (undertaken by ASTM Subcommittee E24.07) indicated a significant range in fracture toughness values depending on the procedure used for evaluating fracture toughness. The fracture toughness for the developmental materials was determined by the Vickers indentation method. At this time the values obtained for fracture toughness can at best only be taken as an indication of the relative toughness of the developmental materials due to their limited testing exposure.

The density, Young's modulus, and Poisson's ratio, are used to calculate the elastic wave velocities. The longitudinal wave velocity, c_L , and the shear wave velocity, c_S , were obtained from the following relations:

$$c_L^2 = \left(\frac{E}{\rho} \right) \frac{1-\nu}{(1+\nu)(1-2\nu)} \quad (4.1)$$

$$c_S^2 = \left(\frac{E}{\rho} \right) \frac{1}{2(1+\nu)} \quad (4.2)$$

The parenthetical values for Poisson's ratio in Table 4.1 indicate that these values have not been measured but are only estimated values.

The fracture threshold can be expressed in terms of the water drop impact velocity required to initiate fracture in the target material. This critical impact velocity, v_{FT} , depends on the size of the drop used and its condition (for example, the level of distortion and impingement angle) prior to impact. If the impact conditions are well-defined and controlled, the fracture threshold is then directly related to the material properties and surface finish of the target material. Evans, Ito, and Rosenblatt (1980) derived an expression for estimating the fracture threshold velocity for spherical projectile impacts.

$$v_{FT}^3 = \frac{2.8 K_c^2 c_R}{\rho_p^2 c_p^2 d_p} \quad (4.3)$$

The fracture toughness for the target material is the dominant material property. The velocity, c_R , is the Rayleigh wave velocity for the target material. In view of the general lack of measured values of v for developmental materials, c_s is used in place of c_R in Eq. (4.3) which introduces a relatively minor error (less than 3%) in the value of the fracture threshold velocity. The denominator in Eq. (4.3) contains information pertaining to the impacting water drop: $\rho_p = 1000 \text{ kg/m}^3$ and $c_p = 1500 \text{ m/s}$.

A series of experiments was undertaken to evaluate the fracture threshold velocity in zinc sulfide, zinc selenide, and one form of spinel. The approximate fracture threshold velocity was inferred for a few of the other materials from the available water drop impact data. In general, it is found that the experimentally-determined fracture threshold velocity differs significantly from the predictions obtained from Eq. (4.3). The details of these investigations will be described.

The predictions obtained from Eq. (4.3) are strongly dependent on the fracture toughness of the target material, however the measurement of fracture toughness in ceramics is still being defined. In addition, the scale of the damage produced by water drop impact conditions represents a localized surface phenomenon, so the controlling fracture toughness has to be introduced in terms of the material's microstructure within a small region of the target's surface. This consideration is most significant for the larger grain materials listed in Table 4.1: CVD zinc selenide and MgAl_2O_4 spinel. The transition from single crystal to polycrystalline fracture energies which is relevant to water drop collisions on moderate to large grain materials has been described by Rice, et al, (1978), in terms of the ratio of the flaw depth to grain size.

Several of the results from fracture toughness evaluations for zinc sulfide, zinc selenide, and MgAl_2O_4 spinel are summarized in Table 4.2. The information provided is essentially self-explanatory, however a few additional remarks will be made about the tabulated data. The purpose for reviewing the fracture toughness evaluations is to illustrate some of the factors which influence the determination of a single, well-defined value for the material property designated fracture toughness.

Table 4.2. Summary of Fracture Toughness Evaluations for Zinc Sulfide, Zinc Selenide, and Spinel.

Material	Grain Structure	Hardness (GPa)	Fracture Toughness (MPa m ^{1/2})	Test Method	Number of Tests	Orientation	Source	Remarks
CVD ZnS	10 μ m equiaxed*	$H_V = 1.9$	1.0	Double torsion	Unknown	Not specified	Evans and Charles, 1976	Tested in dry N ₂
	7 μ m dia. x 56 μ m long	-	0.75 \pm 0.01	Modified expanded ring	4	Crack \perp growth direction	Shockey, et al., 1977	
	2 μ m dia x 25 μ m long	$H_V = 2.1$	0.75	Vickers indentation	Unknown	Assume growth plane indented	van der Zwaag, et al., 1980	
	8-10 μ m dia x 60 μ m long	$H_K = 2.39 \pm 0.06$	0.667 \pm 0.036	Double cantilever beam	11	Crack \perp growth direction	Wimmer and Graves, 1977	
			0.88	Double torsion	1	Crack \perp growth direction	Wimmer and Graves, 1978b	Value of K_{IC} outside scatter for double cantilever beam tests
	4-5 μ m dia x 0.25 μ m long	$H_K = 2.46 \pm 0.04$	0.69 \pm 0.07	Double cantilever beam	10	Crack \perp growth direction	Wimmer and Graves, 1978a	
	2.6 μ m dia x 2.15 μ m long	$H_K = 2.53$	0.60 \pm 0.05	Double cantilever beam	5	Crack \perp growth direction	Wimmer and Graves, 1978b	
			1.34 \pm 0.27	Double cantilever beam	6	Crack \perp growth direction		Invalid tests - pre-crack deviated from guide groove
			0.77	Double torsion	2	Crack \perp growth direction		
			0.87	Double torsion	2	Crack \perp growth direction		
			0.68 \pm 0.12	Double cantilever beam	7	Crack \perp growth direction		Guide groove depths increased to 1.4 mm from 1.5 mm in previous, invalid test series
			1.15	Double cantilever beam	3	Crack \perp growth direction		Only valid test results included in determining average K_{IC} for crack \perp growth direction
	1-5 μ m dia x 0.30 μ m long	$H_V = 2.5$	0.95	Vickers indentation	6	Growth plane indented	Evans, 1982a	
HP ZnS	1-5 μ m equiaxed grains	$H_K = 3.54$	0.44 \pm 0.08	Single edge notched beam	2	Crack \perp to hot pressing direction	Kirchener, 1981	
		$H_V = 2.5$	0.6	Vickers indentation	6	Indented on plane \perp to hot pressing direction	Evans, 1982a	
CVD ZnSe	45-57 μ m	-	0.677 \pm 0.041	Single edge notched beam - four point bend	5		Wurst and Graham, 1975	
	18 μ m	$H_V = 1.0$	0.9	Double torsion	Unknown		Evans and Charles, 1976	Tested in dry N ₂
			0.7	Modified double cantilever beam	Unknown		Freiman, et al., 1975	Tested in air at 22°C, 40% rh
			0.62	Modified double cantilever beam	Unknown			Tested in distilled water
			0.33	Least squares fit to fracture as a function of the reciprocal square root of the flaw size	-			Corresponds to single crystal fracture toughness: 0.29 MPa m ^{1/2}
MgAl ₂ O ₄ (Spinel)	30 to 200 μ m Avg. 90 μ m	$H_V = 0.93$	0.35	Vickers indentation	5		Evans, 1982a	K_{IC} values ranged from 0.25 to 0.6 MPa m ^{1/2}
	Single crystal	$H_V = 16$	1.7		Unknown		Evans and Wilshaw, 1976	
	Single crystal	$H_V = 16$	1.3	Double torsion	Unknown		Evans and Charles, 1976	Tested in dry N ₂
	Single crystal: (100)		1.18 \pm 0.05	Controlled flaw, three point bend	Unknown		Stewart and Bradt, 1980a	
	Single crystal: (110)		1.54 \pm 0.08				Stewart, Iwasa, and Bradt, 1981	
	Single crystal: (111)		1.0 \pm 0.06					
	Polycrystalline		1.90 \pm 0.07				Stewart and Bradt, 1980b	Fracture both intergranular and transgranular
	Polycrystalline		1.16 \pm 0.05				Stewart, Iwasa, and Bradt, 1981	Fracture intergranular

* The grain size reported to be 30 μ m in Evans and Wilshaw (1976), however in a communication with Dr. Evans (Evans, 1979) the grain size was restated as being 10 μ m with equiaxed grains. Representatives from Raytheon Corp. do not recall producing equiaxed grain material and have only been able to achieve a minimum average aspect ratio of about 3 with the CVD process.

The grains in CVD ZnS are significantly elongated in the growth direction with the average grain diameters in the growth plane ranging from about 3 to 10 μm . The growth plane was the surface impacted in the water drop impact experiments, so the appearance of the interactions with the grains on this surface would be similar to a moderately small grain material. Almost all of the fracture toughness measurements for ZnS in Table 4.2 are for this grain orientation. The measured values of K_{IC} show reasonable consistency: ranging from 0.60 to 1.0 $\text{MPa m}^{1/2}$. Wimmer and Graves (1978b) evaluated K_{IC} for cracks propagating perpendicular to the growth direction and found the fracture toughness more than doubled the value obtained for cracks propagating parallel to the growth direction using the double cantilever beam configuration. Unfortunately the pre-crack deviated from the guide groove for this test condition thereby invalidating the K_{IC} measurements. The side grooves were cut deeper which provided a limited number of valid tests. However, when the double torsion test was used, apparently valid measurements were obtained, but the magnitude of the difference in K_{IC} for the two grain orientations was not as dramatic. A single comparison with the materials tested previously indicated that the measurements from the double torsion test were higher than those from the double cantilever beam test configuration. These effects require further investigation before any meaningful conclusions can be reached.

Freiman, et al. (1975), demonstrated the susceptibility of CVD ZnSe to reduced fracture resistance when in a wet environment: water-activated slow crack growth. The effects of the environment on the fracture behavior of CVD ZnSe were also evaluated by Evans and Johnson (1975). By examining the fracture origins, Freiman and his co-workers were able to show that the initial flaw propagated at a fracture toughness level corresponding to the value for a single crystal rather than for a polycrystalline material. Thus in larger grain materials, such as CVD ZnSe with a grain size on the order of 70 μm , failure is initiated from flaws within one or two larger grains. The single crystal fracture energy is therefore more relevant. The direct measurement of K_{IC} for CVD ZnSe using the indentation method supports this result (Evans, 1982a). The K_{IC} values ranged from 0.25 to 0.60 $\text{MPa m}^{1/2}$ indicating the dependence on the grain dimensions at the site of the indent. The enhanced slow crack growth in a water environment measured by Freiman, et al.

(1975), and Evans and Johnson (1975) for CVD ZnSe was also found to be the case for CVD ZnS (Evans, 1982b).

It is interesting to note that the K_c values obtained using a Vickers indentation are quite close to the single crystal fracture toughness determined by Rice, et al. (1978). The cracks produced by the Vickers indent were on the order of 150 μm , so the flaw size is quite close to the grain size. The grain size in CVD ZnSe is quite variable from one region of a single plate to another and from one lot of material to another. Since this is the case and in view of the relative flaw size/grain size dimensions, a correspondingly large variation in the fracture toughness values would be expected. The appropriate value of K_c would have to be determined on an individual basis.

Bradt, and his co-workers (Stewart and Bradt, 1980a, 1980b, Stewart, Iwasa, and Bradt, 1981), have provided a summary of the fracture toughness measurements of MgAl_2O_4 spinel. Again both single crystal and polycrystalline values are provided which is a factor in the water drop impact behavior due to the comparative dimensions of the flaw size and the grain size. The intergranular fracture response in the material with $K_c = 1.16 \text{ MPa m}^{1/2}$ corresponds to one of the materials included in the water drop impact damage evaluation.

A series of hot-pressed MgAl_2O_4 with various percentages of LiF as a pressing aid were obtained for exposure to water drop impacts in order to evaluate the effect of these additions on the water drop impact response. These spinels were prepared by liquid-phase pressure sintering containing 0, 2, 5, and 11 w/o LiF. Fracture toughness values could only be obtained using the indentation method due to the limited supply of material available. Valid fracture toughness could not be obtained due to the inherent grain boundary characteristics of these materials which prevented suitable cracks from developing as the Vicker indenter was loaded for the fracture toughness measurements. The response of these spinels was controlled by the prevailing grain boundary weakness.

4.3 SPECIMEN PREPARATION PROCEDURES

The quality of the specimen's surface has a strong influence on the extent of the damage produced by the water drop collision. It is necessary to carefully prepare the surfaces in order to obtain a realistic evaluation of the material's particle impact resistance. Minimization of the near-surface initial polishing damage is imperative, since the magnitude of the applied stresses generated during the impact process are quite high and these stresses can interact with extremely small flaws (Adler, 1979b). Microscopic examination of the water drop impacted surfaces quickly reveals when the fractures initiated at surface and subsurface scratches. Thus the specimen preparation procedure is an important aspect of the water drop impact damage assessment.

An extensive effort has been under way to develop polishing procedures which will produce acceptable surfaces for the water drop impact experiments. In most cases acceptable surfaces have been obtained, but a substantial amount of time and experimentation were required to achieve satisfactory results.

4.4 TEST CONDITIONS

The materials obtained for this program included both developmental and commercially-available materials. The GE developmental materials consist of four polycrystalline ceramics and one glass. The water drop impact conditions had to be carefully selected, since essentially only one impact could be obtained on materials for which only one specimen was supplied: germania mullite and the four different formulations of yttria zirconia. The limited quantity of the GE developmental materials supplied to ETI for the water drop impact damage assessment was not sufficient for more than a straight-forward comparative screening evaluation. In some cases the specimen dimensions were not adequate to withstand the forces imposed on the specimen in the ETI liquid drop impact facility. A specimen thickness of 5 mm or greater is generally adequate. The diameter of the specimen is not as critical, however to avoid the influence of edge effects a minimum diameter of 15 mm is desirable. Reference to Table 4.1 indicates that these requirements were only marginally satisfied.

In order to evaluate the relative water drop impact resistance for these materials, test conditions had to be selected which produce an observable amount of damage on all of the candidate materials in a particular class of materials. Two categories of materials were considered: higher strength ceramics and glasses.

A 3.2 mm water drop impacting at 762 ms^{-1} (2500 fps) was selected as the impact condition for evaluating the relative water drop impact resistance for the higher strength ceramic materials based on prior experience. This impact velocity is at least twice that predicted for the maximum fracture threshold impact velocity in Table 4.1. The objective was to use an impact condition which would be sufficiently above the fracture threshold that the fractures are fairly well developed but not so severe that specimen cracking would result. In some cases the specimen's thickness was not sufficient to avoid cracking. Table 4.3 summarizes the test conditions for the higher strength ceramics. Pyroceram was introduced as a production material to which the impact response of some of the higher strength ceramics could be compared. A hot-pressed spinel was also included in this test series for comparison with an alternative developmental material.

Due to the lower fracture toughness values for the glass specimens (Table 4.1) a 2.25 mm water drop was selected at an impact velocity of 366 ms^{-1} (1200 fps) as a common impact condition for these materials. In this case magnesium fluoride (although not a glass) is introduced for comparison as a representative infrared window material. The fracture toughness value for magnesium fluoride falls within the range for the various glasses. Table 4.4 lists the test conditions for the glass series.

4.5 RESULTS

The relative magnitude of the water drop impact damage observed on the surfaces of the materials listed in Table 4.1 will be estimated in order to establish the relative water drop impact resistance of these materials. More detailed investigations of the impact damage are warranted, however complete characterization of the surface and subsurface damage for all the materials in Table 4.1 was too time consuming to be included within the scope of this program. More detailed examinations of some additional materials including spinel are described in Section 5.

Table 4.3. Water Drop Impact Conditions for Higher Strength Ceramics

Material	Drop Diameter (mm)	Impact Velocity (m/s)	Remarks
Silica Mullite	3.10	762	Specimen cracked
Germania Mullite	3.07	759	
Aluminum Nitride	3.17	742	
Yttria Zirconia-Z6	3.27	774	
Pyroceram-fortified	3.23	803	
Spinel-2 w/o LiF (Cerodyne)	3.30	735	No observable damage
Silica Mullite	(3.11)	881	
Aluminum Nitride	3.17	932	
	3.19	561	
	3.30	506	
	3.08	468	Specimen cracked--impacted area lost
	3.34	450	
Yttria Zirconia-Z6	3.24	855	
	3.25	902	
Yttria Zirconia #1	(3.13)	1073	
#2	3.21	932	Specimen shattered
#3	3.03	855	Specimen cracked--impact zone fragments available
Pyroceram-unfortified	3.12	960	Specimen cracked--impact zone fragments available
Pyroceram-fortified	3.19	973	Minor imperfections in water drop

Table 4.4. Water Drop Impact Conditions for Selected Glasses

Material	Drop Diameter (mm)	Impact Velocity (m/s)	Remarks
Germanate Glass	2.31	374	Specimen cracked--impacted area not recovered
Soda Lime Glass Corning 0080	2.24	351	
Borosilicate Glass Corning 7740	2.31	374	
Fused Silica Corning 7940	2.25	361	
Magnesium Fluoride IRTRAN 1	2.32	380	
Germanate Glass	2.30	531	
	3.00	695	
Soda Lime Glass	2.25	462	
	2.29	521	
Borosilicate Glass	2.31	469	
Magnesium Fluoride	2.32	578	

4.5.1 Fracture Threshold Evaluations

The onset of fracture was determined for CVD ZnS, CVD ZnSe, and HP MgAl_2O_4 for nominal 2.30 mm water drops impacting at successively lower velocities. The specimens were very carefully polished in order to minimize the effects of the surface finish on the material's response. The test procedure was to select an impact velocity, impact the specimen, and then examine the impacted surface for water drop impact damage at magnifications from 50 to 400 times.

Maintenance of a narrow tolerance on the impact velocity in the water drop impact facility presents some difficulty for velocities below 200 ms^{-1} . Forty water drop impacts were used to obtain completely documented impact data for CVD ZnS, CVD ZnSe, and MgAl_2O_4 . This data included a photograph of the water drop just prior to impact, an impact velocity, and no indication of interactions with surface polishing defects on the specimen's surface. Twenty-four fully documented impacts were obtained. The velocity range for spinel did not present a problem, except that the threshold velocity was overestimated initially. The low velocities for ZnS and ZnSe were the major difficulty.

The fracture threshold was determined by obtaining an upper and lower bound on the velocity at which damage was observed and when it was not observed. The fracture threshold velocities obtained on this basis are:

CVD zinc sulfide	$168 \text{ ms}^{-1} < V_{\text{FT}} < 198 \text{ ms}^{-1}$
CVD zinc selenide	$128 \text{ ms}^{-1} < V_{\text{FT}} < 152 \text{ ms}^{-1}$
HP spinel	$V_{\text{FT}} \leq 408 \text{ ms}^{-1}$

An effort was made to narrow the bounds for zinc sulfide and zinc selenide, however the level of effort required became excessive and so further testing was terminated.

Hackworth and Kocher (1978) found the following ranges for the fracture threshold velocities for CVD ZnSe and CVD ZnS for single 2 mm water drop impacts:

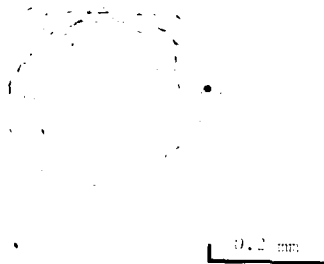
CVD zinc sulfide	$V_{\text{FT}} \leq 175 \text{ ms}^{-1}$
CVD zinc selenide	$137 \text{ ms}^{-1} < V_{\text{FT}} < 152 \text{ ms}^{-1}$

This data is consistent with the previous results except that the above values of V_{FT} should be slightly higher due to the difference in the nominal drop diameters: 2.25-2.30 mm compared with a 2.0 mm diameter drop. The presence of impact damage was determined using optical microscopy.

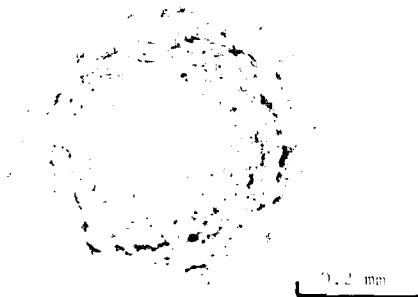
The experimental values of V_{FT} do not agree with the predicted values recorded in Table 4.1 for 2.25 mm drop diameters. In addition, due to the large grain size in CVD ZnSe and spinel, an impact condition is reached where the dimensions of the fracture are on the order of a single grain or less. Near the fracture threshold velocity the fractures in CVD ZnSe are a mixture of both intergranular and transgranular cleavage. At this point the single crystal values of K_C are more appropriate. Based on the available data (Table 4.2) this effect may not be too significant for spinel where the single crystal and polycrystalline K_C values are comparable, but it is quite significant for CVD ZnSe. Using a single crystal value of $K_C = 0.3 \text{ MPa m}^{1/2}$ yields a fracture threshold velocity $V_{FT} \approx 50 \text{ ms}^{-1}$ for a 2.25 mm drop. On this basis the discrepancy between the experimental and calculated fracture threshold velocities indicates more strongly that the correlation in Eq. (4.3) is not properly representing the physical features of fracture initiation due to soft body impingement. Additional inconsistencies utilizing Eq. (4.3) will be cited in Sections 4.5.2 and 4.5.3.

A small quantity of HP ZnS (IRTRAN 2) was available and was used to compare the extent of the damage in this material with that for CVD ZnS. A comparison of roughly equivalent impact conditions for CVD ZnS, HP ZnS, and CVD ZnSe are shown in Fig. 4.1. Although CVD ZnSe displays the worse water drop impact resistance, it should be noted that it was impacted by a slightly smaller drop than the other two materials: the fracture depths could therefore be somewhat greater than shown in Fig. 4.1c. The water drop impact resistance of HP ZnS appears to be comparable to the water drop impact resistance of CVD ZnS. This result is fairly consistent with the lower fracture toughness values reported for the HP ZnS (Table 4.2). Additional tests on HP ZnS are required to substantiate the relative water drop impact resistance determined for these two forms of ZnS.

- (a) 2.32 mm Water Drop
Impact on CVD ZnS at
 198 ms^{-1} .



- (b) 2.33 mm Water Drop
Impact on HP ZnS at
 199 ms^{-1} .



- (c) 2.21 mm Water Drop
Impact on CVD ZnSe at
 197 ms^{-1} .

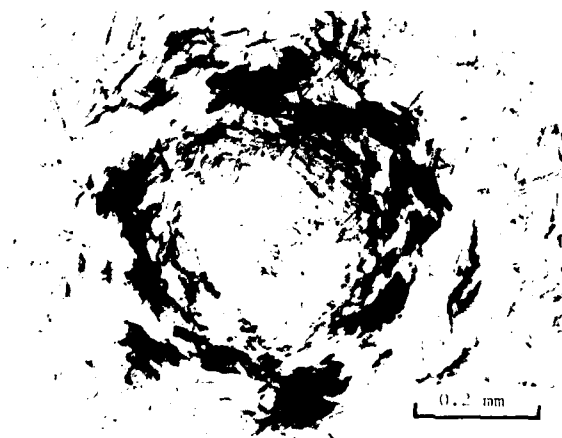


Figure 4.1. Comparison of Extent of Water Drop Impact Damage on Zinc Chalcogenides for Impact Velocities Slightly Above Fracture Threshold Levels.

In order to obtain at least some quantitative evaluation of what the actual difference in the water drop impact resistance for these two materials as well as CVD ZnSe may be, the subsurface fractures were measured for the higher velocity impact conditions listed in Table 4.5. These measurements are compared with the corresponding fracture measurements for CVD ZnS (described in Section 2) in Fig. 4.2-4.4.

The influence of the larger grain size in CVD ZnSe (compared with ZnS) on the surface and subsurface fracture morphology is evident in Fig. 4.5. The general features of the fractures are the same as have been already described for ZnS (Adler and James, 1980). The onset of radial fractures and their horizontal fractures below the central undamaged zone occur at an impact velocity (for 2.25 mm drops) roughly 100 ms^{-1} lower in CVD ZnSe than CVD ZnS. A greater degree of variation in the dominant Type I and Type II fractures is also observed for impact velocities above 350 ms^{-1} . This tendency is clearly noted in the data recorded in Fig. 4.2-4.4.

The fracture measurements for HP ZnS (shown in Fig. 4.2-4.4) are quite consistent with the general trends in the measurements for CVD ZnS. At most, HP ZnS, based on very limited data, is only marginally less water drop impact resistant than CVD ZnS. The detailed microscopic features of the low velocity (near the threshold) multiple water drop impact damage in CVD ZnS, HP ZnS, and CVD ZnSe have been described previously by Adler and Hooker (1978).

4.5.2. Higher Strength Ceramics

Pyroceram (Corning 9606) and a spinel were introduced for comparison with the impact response of the higher strength ceramics. Both a fortified and unfortified form of Pyroceram were obtained for evaluation. The surface fortification procedure for Pyroceram used by Corning Glass Works is to place it in boiling sodium hydroxide. The material is washed and the procedure repeated several times. This process tends to round out the crack tips of surface flaws to a depth of approximately 150 to 225 μm . This treatment is a practical approach for providing a reasonable surface condition for most radome applications. Alternatively the flaws in the as-received

Table 4.5. Water Drop Impact Conditions and Subsurface Fracture Measurements for CVD ZnSe and HP ZnS.

Material	Shot No.	Impact Velocity (ms ⁻¹)	Drop Diameter (mm)	2a _c (mm)	Type I Fractures		Type II Fractures	
					Location (mm)	Depth (mm)	Location (mm)	Depth (mm)
CVD ZnSe	1300	387	2.26	0.36	0.32	0.38	0.59	0.48
	1326	515	2.08	.45	.46	.65	.68	.55
	1331	540	2.03	.40	.48	.95	.83	.93
CVD ZnSe	1468	415	2.31	0.44	0.39	0.55	1.02	0.45
	1467	420	2.20	.33	.37	.64	1.08	.43
	1463	485	2.36	.45	.46	.59	0.93	.62
	1464	504	2.36	.40	.37	.95	1.16	.78
HP ZnS	1485	404	2.21	0.35	0.31	0.26	0.55	0.40
	1507	517	2.30	0.35	.32	.58	.65	.53

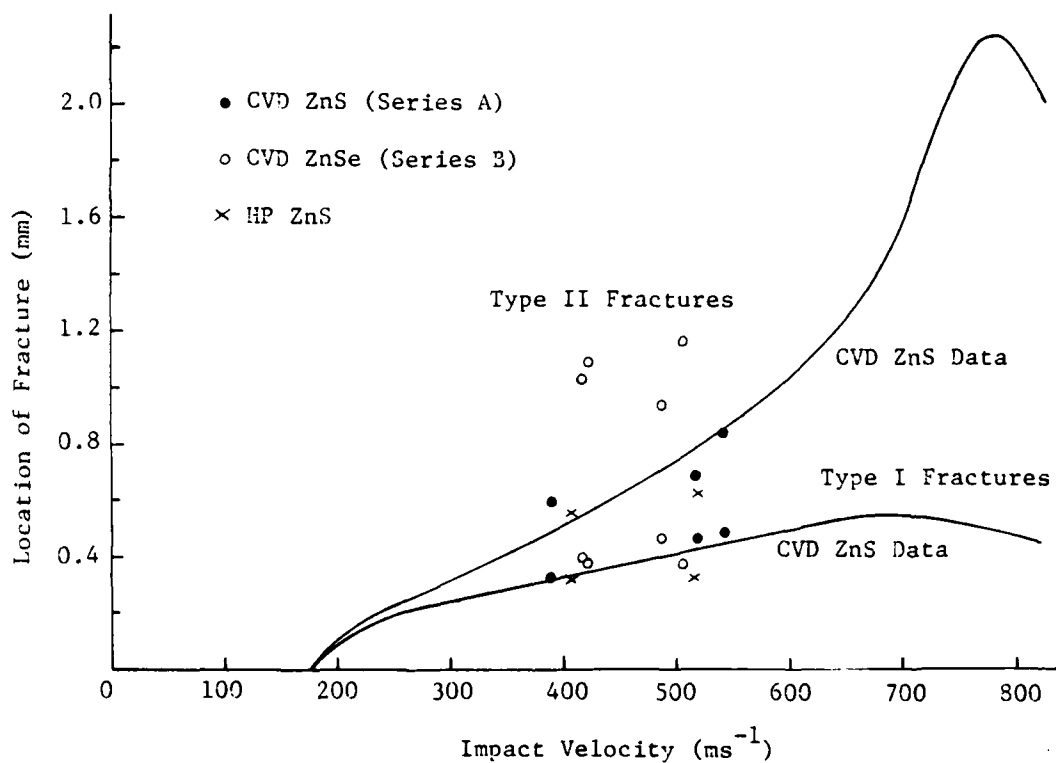


Figure 4.2. Radial Distance to Dominant Type I and Type II Fractures as a Function of Impact Velocity for Water Drop Impacts on CVD ZnSe and HP ZnS Compared with CVD ZnS Data.

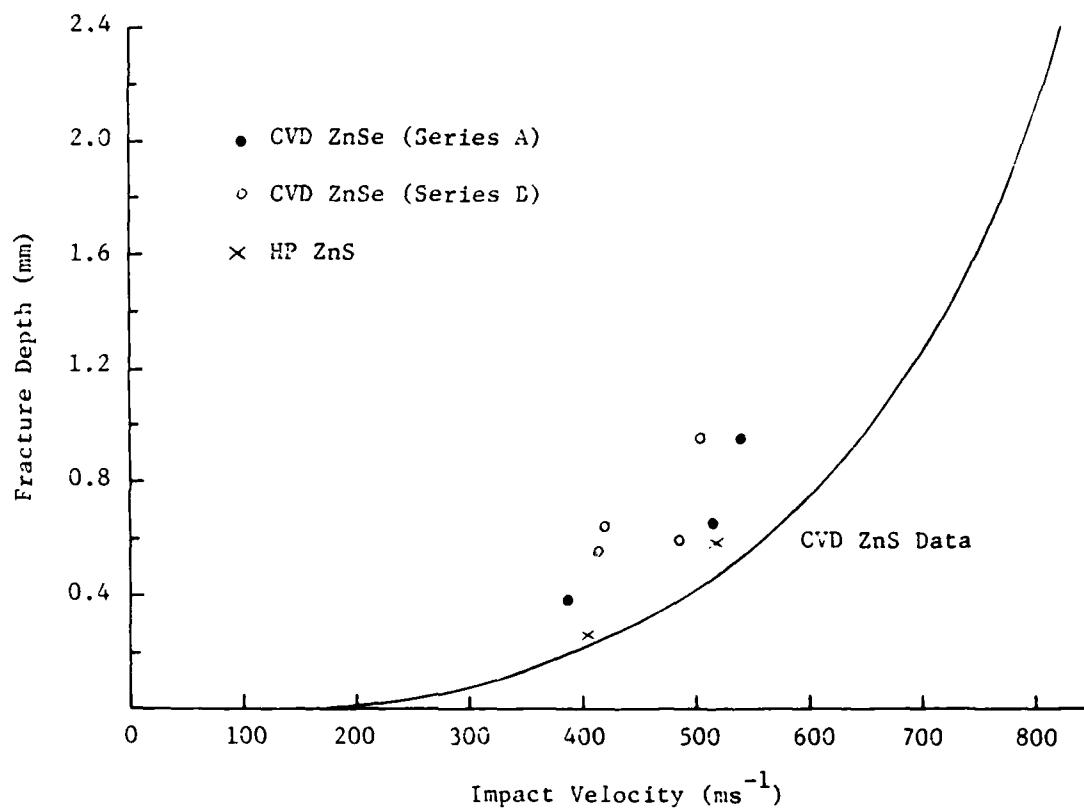


Figure 4.3. Penetration Depth for Type I Fractures as a Function of Impact Velocity for Water Drop Impacts on CVD ZnSe and HP ZnS Compared with CVD ZnS Data

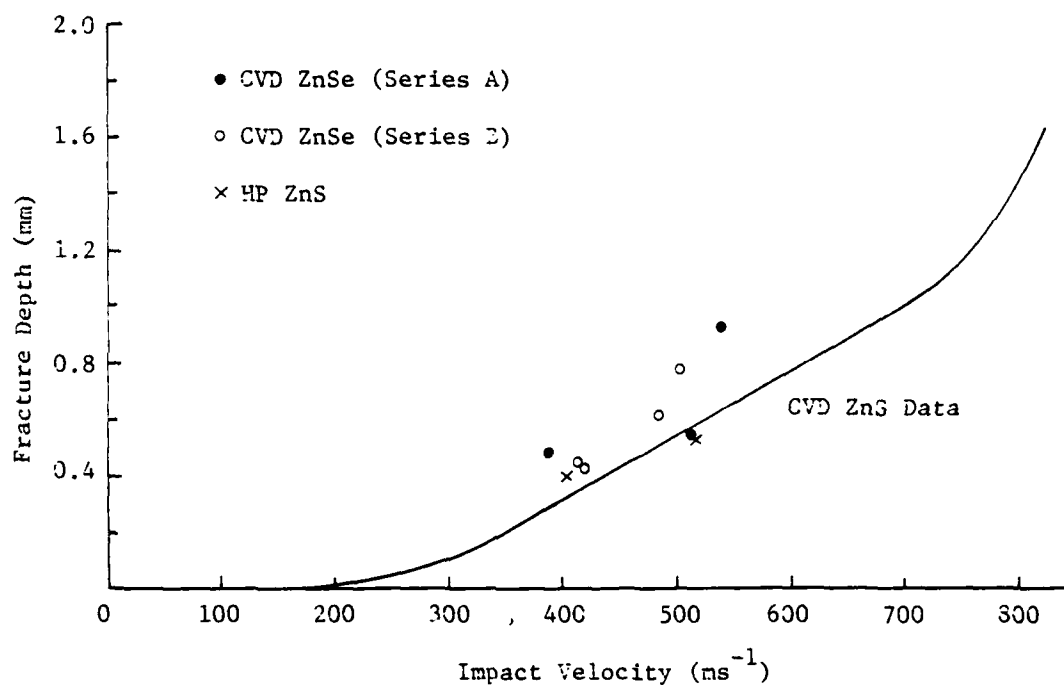


Figure 4.4. Penetration Depth for Type II Fractures as a Function of Impact Velocity for Water Drop Impacts on CVD ZnSe and HP ZnS Compared with CVD ZnS Data.

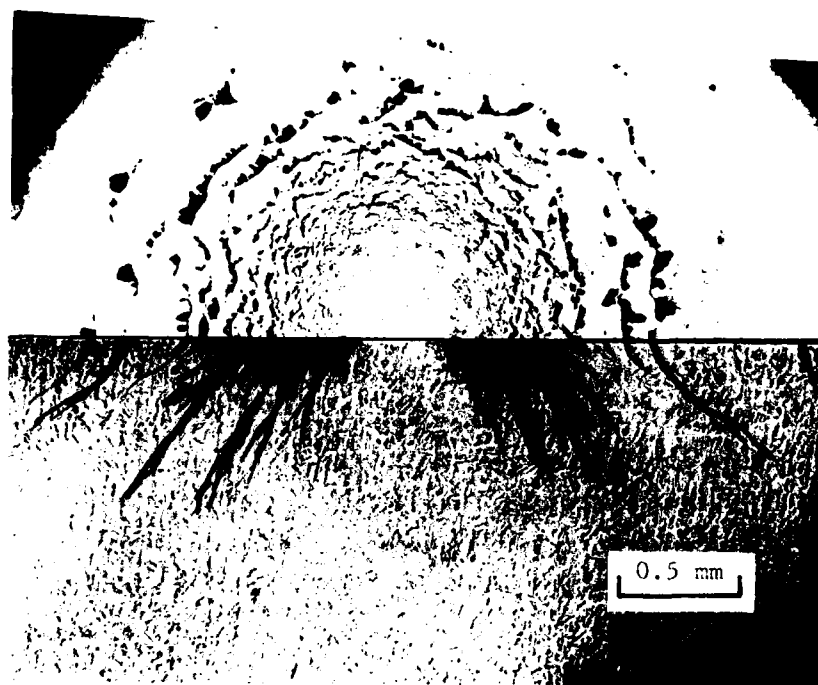


Figure 4.5. Subsurface Fracture Pattern for CVD ZnSe. Impact Condition is a 2.30 mm Water Drop Impacting at 420 ms^{-1} .

surface of the unfortified Pyroceram can be minimized by polishing the surface. This obviously is a tedious procedure for production radomes, however the influence of the finishing process on the water drop impact response is of interest. The effect of the surface treatment on the water drop impact damage is illustrated below.

The first series of tests in Table 4.3 provides a comparison of the extent of the impact damage on each material for a nominal 3.2 mm water drop impacting at 760 ms^{-1} . The nature of the damage is somewhat different for the spinel and fortified Pyroceram compared with the fine-grained developmental materials. The extent of the damage in each of these cases is shown in Fig. 4.6 to 4.7.

The character of the water drop impact damage was found to be quite distinct for fortified and unfortified Pyroceram. The polished untreated material displays a fracture pattern which is in conformity with small-grained polycrystalline ceramics. (Unfortunately this water drop impact is only of fair quality.) The circumferential fracture array (Fig. 4.8a) is characteristic of all of the materials listed in Table 4.1. However the same nominal impact conditions produced a distinctly different type of damage in the fortified Pyroceram. The damage site shown in Fig. 4.8b consists mainly of deformation and relatively little crack initiation. The damage is reasonably contained in the deformed annulus. There is no evidence of additional damage beyond that associated with the annular region. The higher velocity impact in Fig. 4.8b produced considerably more damage but it is still contained within a well-defined annular zone.

In contrast to the observations of the damage modes in Pyroceram, spinel, due to its large grain size (an average grain size of $60 \mu\text{m}$), shows a strong tendency for grain disruption and grain pull-out (Fig. 4.7a). The extent of the surface disruption is therefore quite dramatic. An expanded discussion of water drop impact damage in spinel is presented in Section 5.2.

The GE developmental materials have a very small grain size (less than $1 \mu\text{m}$) so well-defined circumferential fracture arrays are characteristic for these materials. Roughly comparable levels of damage are observed in



a. 3.17 mm Water Drop Impact
on Aluminum Nitride at
 742 ms^{-1} .

0.5 mm



b. 3.10 mm Water Drop Impact
on Silica Mullite at
 762 ms^{-1} .

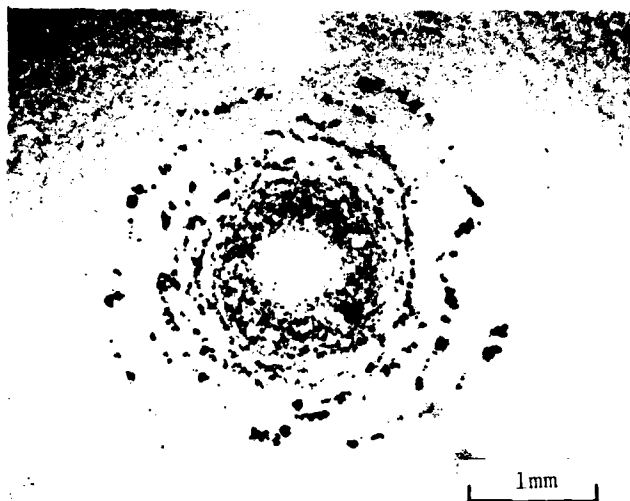
0.5 mm



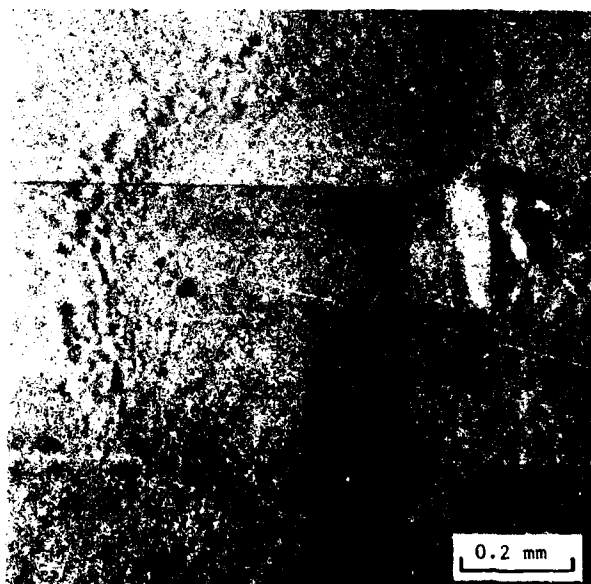
c. 3.07 mm Water Drop Impact
on Germania Mullite at
 759 ms^{-1} .

0.5 mm

Figure 4.6. Comparison of Water Drop Impact Damage on Aluminum Nitride, Silica Mullite, and Germania Mullite.

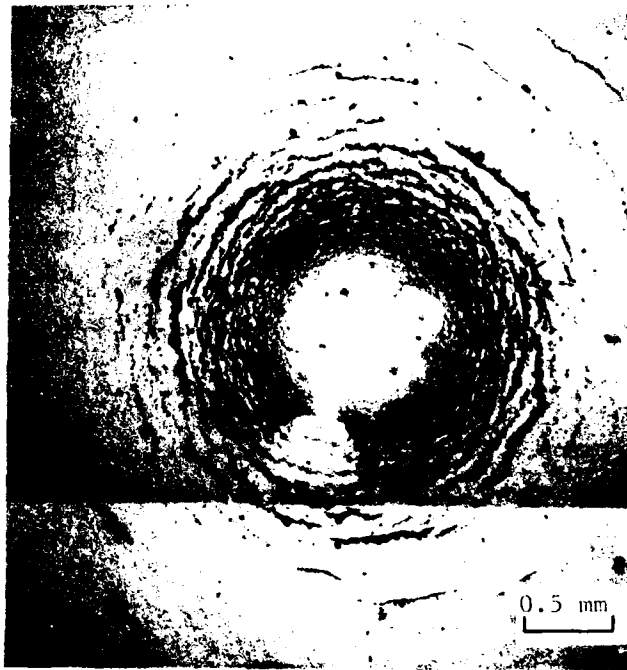


a. 3.30 mm Water Drop Impact on Spinel at 735 ms^{-1} .

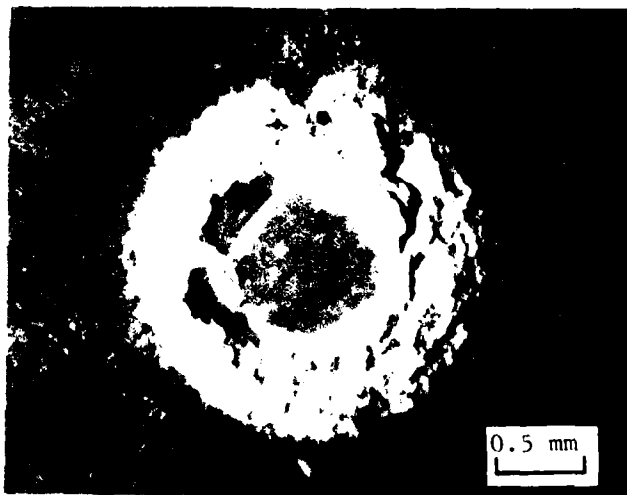


b. 3.23 mm Water Drop Impact on Fortified Pyroceram at 803 ms^{-1} .

Figure 4.7. Water Drop Impact Damage on Spinel and Pyroceram.



a. 3.12 mm Water Drop Impact on Unfortified Pyroceram at 960 ms^{-1} (Polished Surface)



b. 3.19 mm Water Drop Impact on Fortified Pyroceram at 973 ms^{-1}

Figure 4.8. Higher Velocity Water Drop Impacts on Unfortified and Fortified Pyroceram.

the germania mullite, silica mullite, and aluminum nitride specimens. No damage (fracture) whatsoever was observed on the yttria zirconia Z6 specimen. From the overviews in Fig. 4.6-4.7 the water drop impact resistance of this selection of ceramic materials would be in decreasing order: yttria zirconia, fortified Pyroceram, aluminum nitride, silica mullite, germania mullite, spinel. This superficial comparison is only an indication of the relative ranking. A more definitive comparison would be based on an examination of the nature and extent of the subsurface fractures and the subsequent growth of the initial fractures due to multiple water drop collisions.

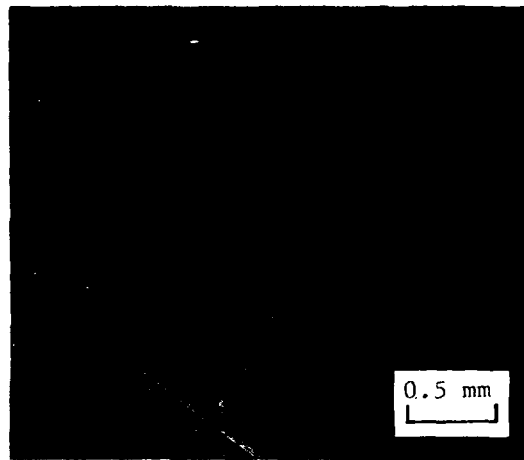
The absence of any observable damage on the initial yttria zirconia specimen was the basis for a decision to increase the impact velocity for the remaining yttria zirconia specimens. However, due to the minimal thickness for these specimens, they did not survive the imposed impact conditions. One specimen was fired at a velocity 200 ms^{-1} higher than desired and was completely destroyed. The velocities for the remaining two yttria zirconia specimens were based on the results for Z6, but these particular materials were not as strong. The fragments recovered contained damage which was significantly greater than that for material Z6 at comparable impact conditions.

The additional impacts on aluminum nitride and yttria zirconia Z6 establish that the fracture threshold for aluminum nitride is roughly 460 ms^{-1} while it is around 850 ms^{-1} for yttria zirconia Z6. This experimental result is completely contrary to the calculated fracture threshold velocities in Table 4.1.

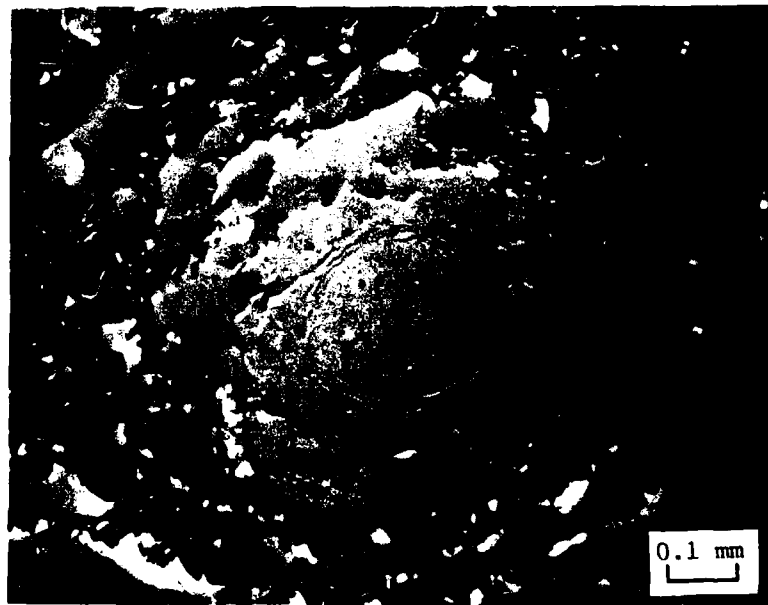
4.5.3. Glasses

A number of ceramics with considerably lower fracture threshold velocities were also evaluated for their relative water drop impact resistance. The impact conditions are summarized in Table 4.4.

The differences in the fracture arrays for the four materials in which damage resulted for impacts around 360 ms^{-1} can be seen in Figs. 4.9 to 4.11. All the glasses have a very distinct circular boundary surrounding



a. Overview of Damage Site.

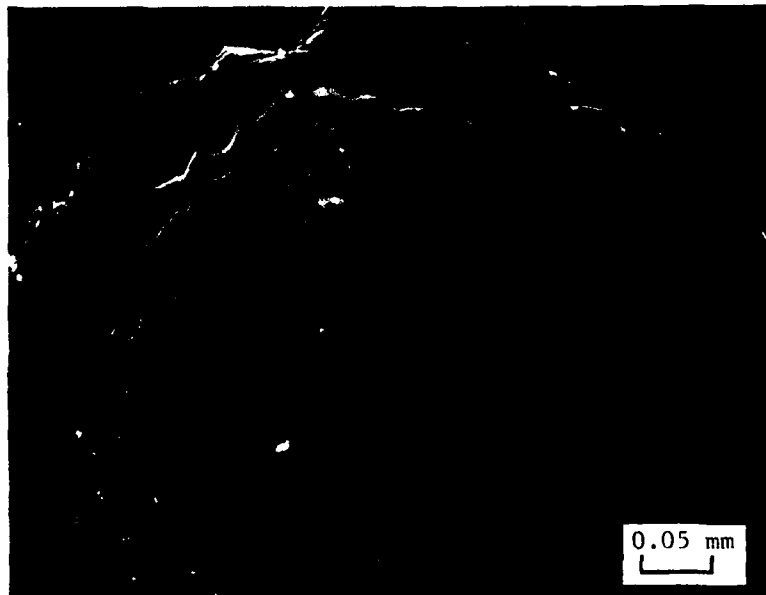


b. Detail of Central Region of Impact Damage Site

Figure 4.9. 2.25 mm Water Drop Impact on Fused Silica at 361 ms^{-1} .



a. Overview of Damage Site.

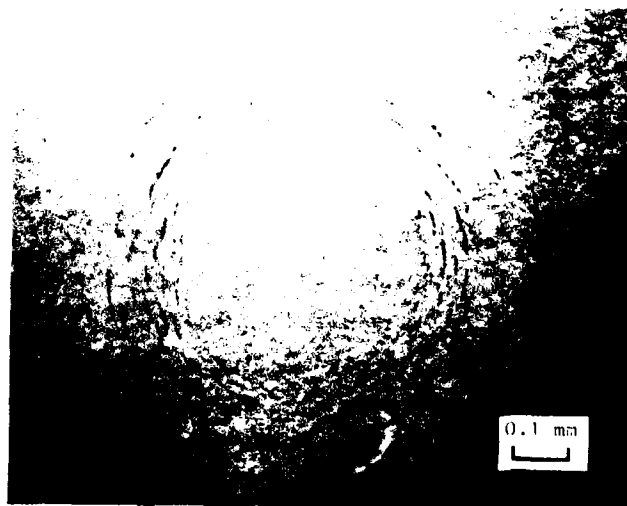


b. Detail of Central Region of Damage Site.

Figure 4.10. 2.31 mm Water Drop Impact on Borosilicate Glass at 374 ms^{-1} .



a. 2.31 mm Water Drop Impact on Germanate Glass at 374 ms^{-1} .



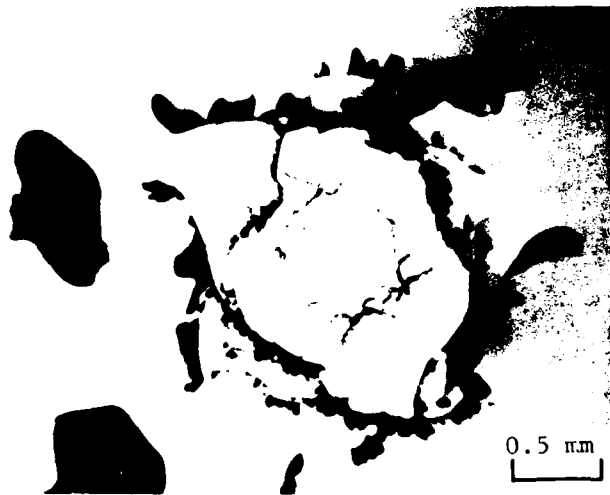
b. 2.32 mm Water Drop Impact on Magnesium Fluoride at 380 ms^{-1} .

Figure 4.11. Comparison of Water Drop Impact Damage on Germanate Glass and Magnesium Fluoride.

the central undamaged zone which is the inner diameter of an annulus of very shallow circumferential fractures. This fracture annulus is typically observed in materials such as ZnS only after they are etched. The notable feature of these inner fracture annuli is that the diameter of the central undamaged zone varies considerably for each glass, even though the impact condition was essentially held constant. The diameter of the central undamaged zone is 0.35 mm for germania glass, 0.26 mm for borosilicate glass, and 0.23 mm for fused silica. The magnesium fluoride would have to be etched to obtain an accurate estimate of the diameter of the undamaged zone: the diameter for the unetched specimen is 0.42 mm.

Although the results from the fracture threshold computation, Eq. (4.3), recorded in Table 4.1 indicate that the germanate glass should have superior impact resistance compared with soda lime glass, borosilicate glass, and fused silica and that the response of the latter three glasses should be comparable, this was not the case. Soda lime glass was the most impact resistant while fused silica has the worst water drop impact resistance by a considerable degree. No water drop impact data was observed in soda lime glass at 351 ms^{-1} which is therefore below the fracture threshold, while the fracture threshold for fused silica is estimated to occur at an impact velocity possibly more than 100 ms^{-1} lower than this velocity. The fracture threshold for soda lime glass is much higher than previously found for this material. The difference could be due to the quality of the polished surface being achieved at the present time. The comparisons described here for the glass specimens appear to be for polished surfaces of comparable quality. The impact resistance of the germanate glass was significantly less than soda lime glass but slightly better than borosilicate glass. However the large fractures accompanying the circumferential fractures in borosilicate glass (Fig. 4.10) makes a direct comparison difficult with a material which possesses an ordered array of circumferential fractures. The water drop impact resistance of magnesium fluoride was better than germanate glass but appears to have a lower fracture threshold velocity than soda lime glass.

The damage produced at impact velocities higher than the nominal 360 ms^{-1} is shown in Figs. 4.12 to 4.15. The well-defined circular boundary

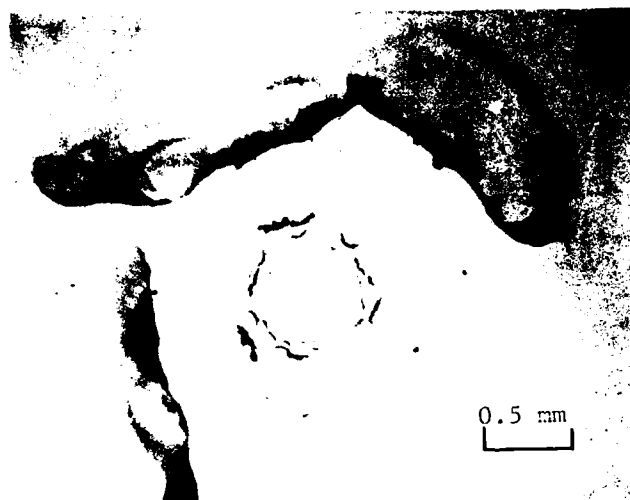


a. Overview of Impact Damage

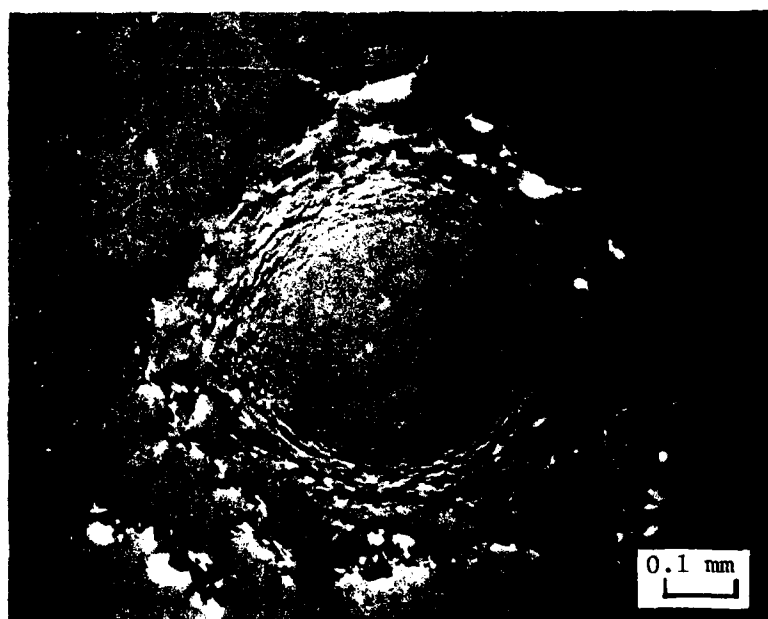


b. Detail of Central Region of Impact Damage Site

Figure 4.12. 2.31 mm Water Drop Impact on Borosilicate Glass at 469 ms^{-1} .

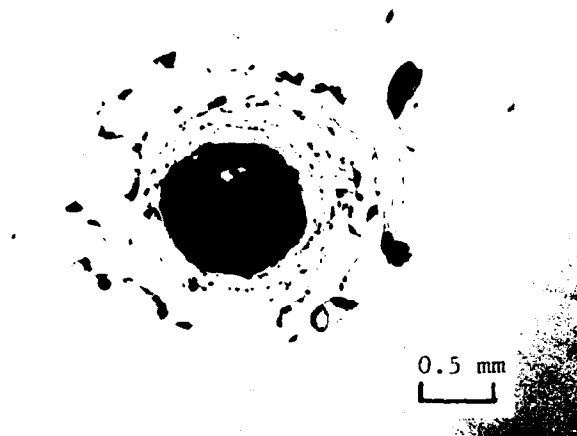


a. Overview of Impact Damage

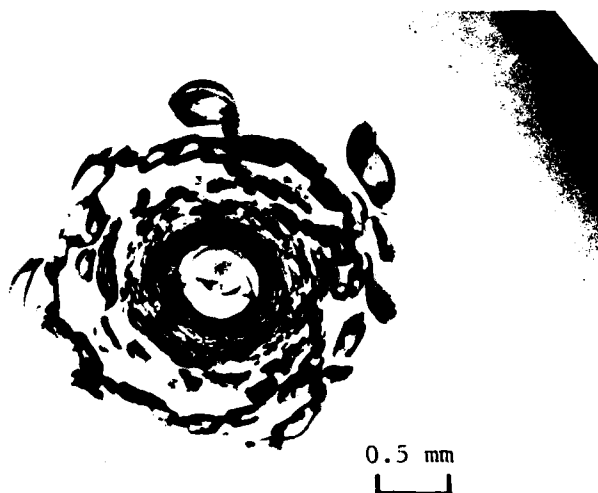


b. Detail of Central Region of Impact Damage Site

Figure 4.13. 2.25 mm Water Drop Impact on Soda Lime Glass at 462 ms^{-1} .



a. Reflected Light Illumination.



b. Transmitted Light Illumination.

Figure 4.14. 2.30 mm Water Drop Impact on Germanate Glass at 531 ms^{-1} .

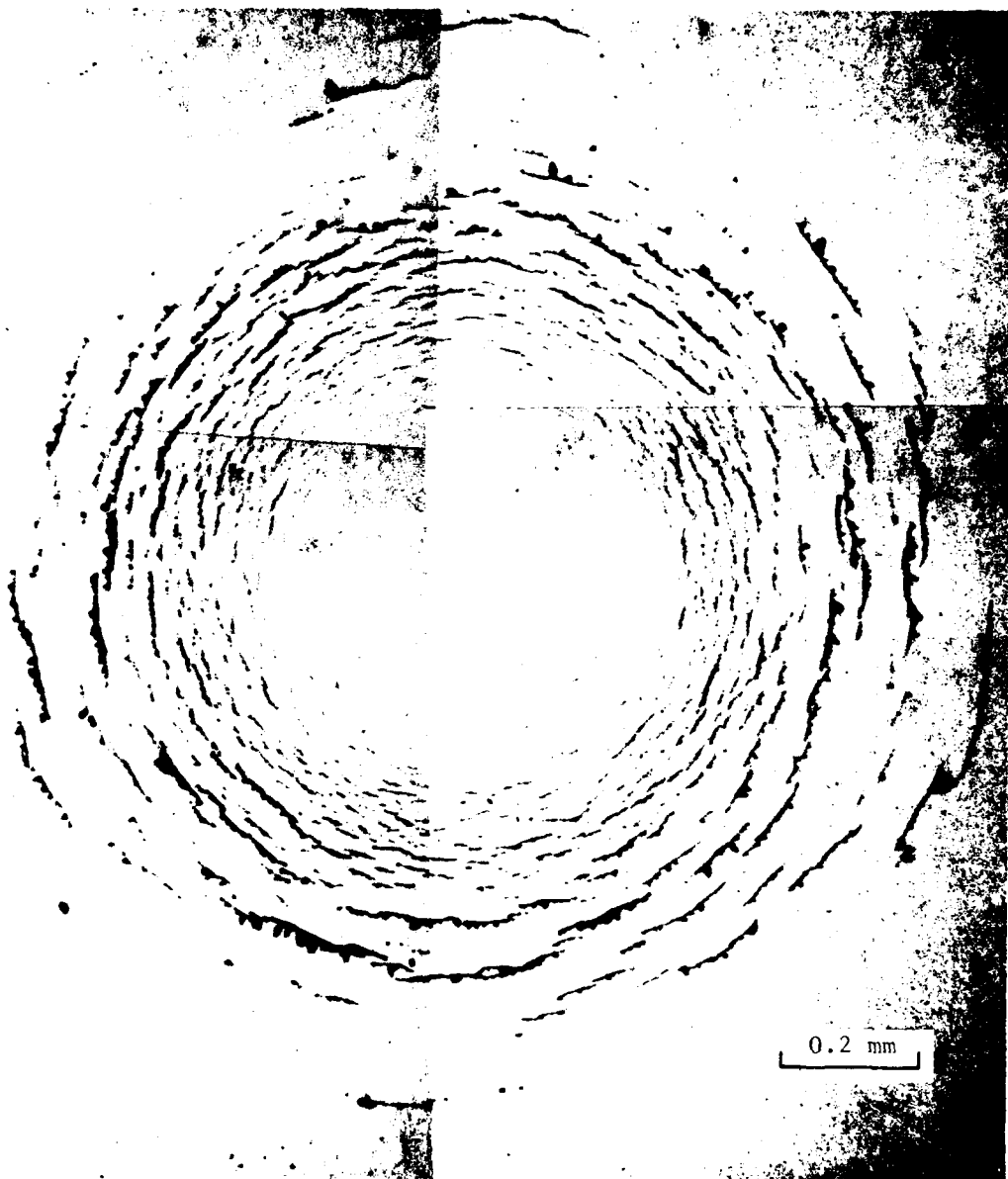


Figure 4.15. 2.32 mm Water Drop Impact on Magnesium Fluoride at 578 ms^{-1} .

surrounding the central undamaged zone persists for borosilicate and soda lime glass (Fig. 4.12 and 4.13). In view of the extent of the damage in fused silica at 360 ms^{-1} , this glass was not subjected to higher velocity impact conditions. The circumferential fracture arrays are seen to be reasonably contained for germanate glass (Fig. 4.14) and magnesium fluoride (Fig. 4.15). The severity of the impact condition for the germanate glass was such that the central region of the impact site was removed, however, magnesium fluoride at a higher impact velocity still maintains its integrity. The damage is an orderly array of circumferential fractures characteristic of small-grain polycrystalline ceramics. On the other hand, the fracture arrays for soda lime and borosilicate glass are quite random outside the circular fracture annulus surrounding the central undamaged zone and a few large fractures dominate the damage produced. For equivalent impact conditions the diameter of this inner boundary is found to be the same for these two glasses: 0.31 mm. The large fractures away from the central site make these glasses impractical to use in a rain environment. The occurrence of large, discrete fractures away from the impact site has been observed for these glasses during several test series. At first, their presence was viewed with skepticism that they were an inherent property of the material but instead related to the test conditions. Enough tests have now been completed for various lots of material to indicate that the large fractures are a characteristic of well-prepared surfaces of soda lime and borosilicate glass subjected to water drop impacts, although a minority of the test results still show that more orderly and contained arrays of circumferential fractures can be achieved. The surface conditions for one form of damage or the other have not been identified.

It is seen that the extent and nature of the impact damage is quite diversified in contrast to the similar fracture response that would be expected for the glass specimens and the definite ordering of the ceramics based on the material properties listed in Table 4.1. Neither fracture toughness nor hardness nor the wave propagation characteristics of the material are sufficient to indicate the onset of water drop impact damage in any of the materials evaluated.

5.0 EXAMINATION OF WATER DROP IMPACT DAMAGED MATERIALS

The water drop impact response of single crystal MgO was examined in some detail in prior work (Adler and James, 1979). It was of interest to investigate how the energy dissipation mechanisms identified for single crystals might apply to polycrystalline MgO. A limited quantity of both chemically vapor deposited (CVD) and hot-pressed (HP) MgO was obtained for this purpose. In addition a limited amount of magnesium aluminate spinel (MgAl_2O_4) was obtained which had varying percentages of LiF used as a pressing aid. In this case the objective of the water drop impact experiments was to evaluate how strongly the influence of LiF on the grain boundaries affects the water drop impact resistance of spinel.

Each of the materials obtained for investigation required a small development effort in order to establish polishing procedures which would produce satisfactory surfaces for the water drop impact experiments, to gain a capability in utilizing etchants when available, and to develop thin sectioning procedures for subsurface fracture characterization. In view of the time required to thoroughly characterize a material sample before and after being impacted by a water drop, some of the materials received presented too many problems in this regard and so they were only examined in a superficial manner. The work done on materials falling into this category is briefly described in Section 5.3.

5.1. MAGNESIUM OXIDE

Plastic deformation has been demonstrated to be a very effective mechanism for impact energy dissipation for MgO single crystals (Adler and James, 1979). It was shown that by introducing numerous active dislocations into the surface of single crystal MgO that fracture initiation could be suppressed at impact velocities in excess of 575 ms^{-1} . Specimens without induced dislocation sources exhibited significant fracturing at velocities as low as 400 ms^{-1} . The presence of the easily motivated dislocations allows dissipation of the impact energy without developing stresses high enough to cause fracture.

It was of interest to investigate how these observations would apply to polycrystalline forms of MgO. Two types of polycrystalline MgO were obtained: IRTRAN 5, a hot-pressed material produced by the Eastman Kodak Company and a CVD processed material produced by the Raytheon Company. Samples of both materials were etched with a 10N solution of sulfuric acid at 50°C. This etchant reveals dislocation etch pits (on most crystallographic planes), grains and subgrain boundaries, and surface flaws after a 10 sec. immersion.

The HP MgO had a very low dislocation content within grains. The dislocations present appear to be the result of the polishing procedure, since the dislocations (regardless of grain orientations) are aligned with the polishing direction. The material is essentially stress free, as determined by polarized light birefringence. Some birefringence was detected in the vicinity of the large inclusions present in the material.

The CVD MgO had a high dislocation content with numerous low-angle, sub-grain boundaries. Polarized light birefringence indicated that there was a significant amount of internal stress within the grains. There is a high concentration of inclusions in this material which are on the order of the smaller grain dimensions. These inclusions are large enough to be readily seen with the unaided eye.

The water drop impact damage on HP MgO is shown in Fig. 5.1 for a 2.04 mm drop impacting at 715ms^{-1} . The observed damage is somewhat similar to that found for CVD ZnS (Adler and James, 1980). The characteristic Type I and Type II fracture morphologies described by Adler and James (1980) are represented to some extent in HP MgO. Quantitative differences between the HP MgO and CVD ZnS are evident, however the non-uniformity in the dominant fracture depths on each side of the central undamaged zone make it difficult to be precise. Noting this lack of uniformity, the location and depth of the dominant fractures appears to be less than half the values found for CVD ZnS (Fig. 2.3 to 2.5).

Observations of impact sites on HP MgO revealed no stress birefringence. In contrast, impacts on single crystal MgO exhibited significant stress birefringence (Adler and James, 1979). Etching of the impact site failed

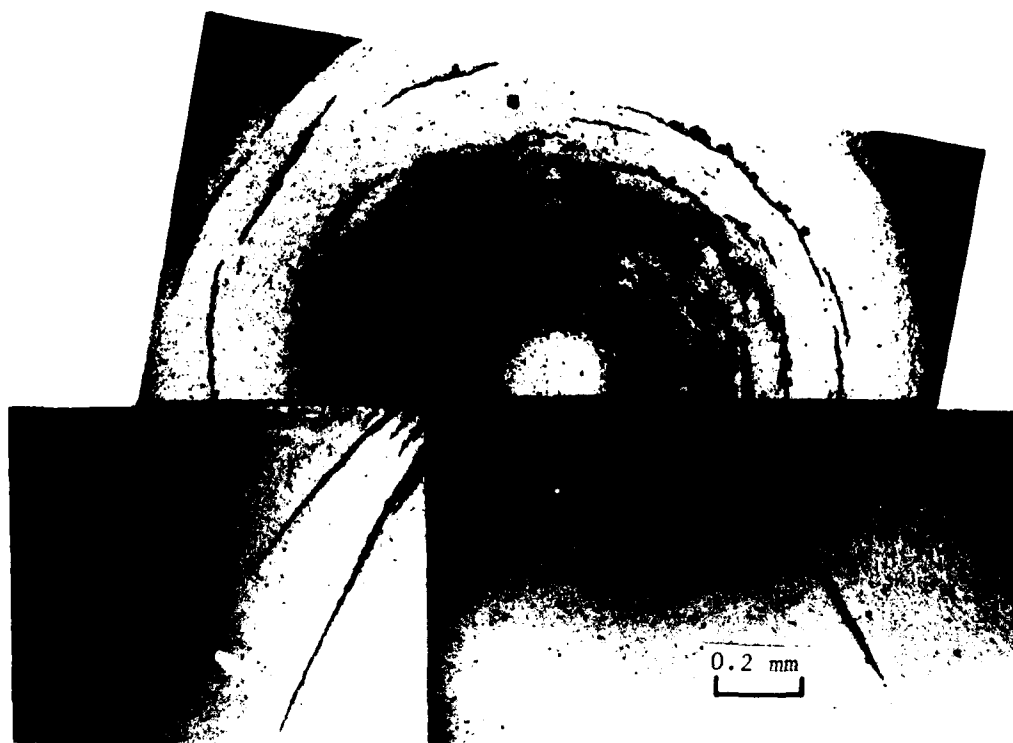


Figure 5.1. Subsurface Fracture Pattern for a 2.04 mm Water Drop Impact on HP MgO at 715 ms^{-1} .

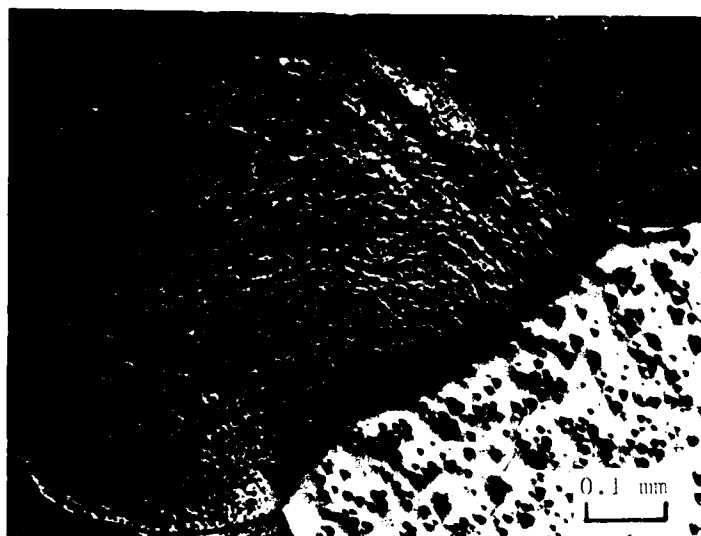
to reveal any dislocation activity resulting from the impact. This is also in direct contrast to the behavior of single crystal MgO which exhibits significant dislocation activity. The fractures produced in HP MgO exist almost exclusively on the grain boundaries. The preference for intergranular fracture is also apparent during rough polishing and microhardness indentation. The primary mechanism of material removal during rough grinding and polishing is grain pull-out. During fine polishing whole grains will occasionally be removed. The relative ease by which the grains are removed, as opposed to portions of grains, indicates that the grain boundaries are a preferred fracture path. It was also observed that whole grains will frequently pop out of the strained region around an indentation site during microhardness evaluations.

CVD MgO was found to be considerably more water drop impact resistant than (001) MgO (Adler and James, 1979) or HP MgO. This result is based on the observation that water drop impacts on CVD MgO at velocities up to 564 ms^{-1} failed to produce any fractures. Due to the thinness (approximately 1 mm) of the available material, the specimens tended to fracture during launching and recovery in the water drop impact facility at velocities above 600 ms^{-1} . After several attempts a successful impact was obtained at 660 ms^{-1} . This impact condition produced limited (100) cleavage fractures within the grains and a small grain boundary fracture. For comparison, the threshold velocity for observable fracture damage in HP MgO is between 330 ms^{-1} (no fracture or dislocations detected) and 520 ms^{-1} (circular fracture patterns were formed). Also for comparison, impacts at 400 ms^{-1} produced dislocations and fractures on (100) faces of low dislocation content single crystal MgO. Thus the fracture suppression mechanism observed for single crystal MgO with induced dislocations was also present in polycrystalline CVD MgO.

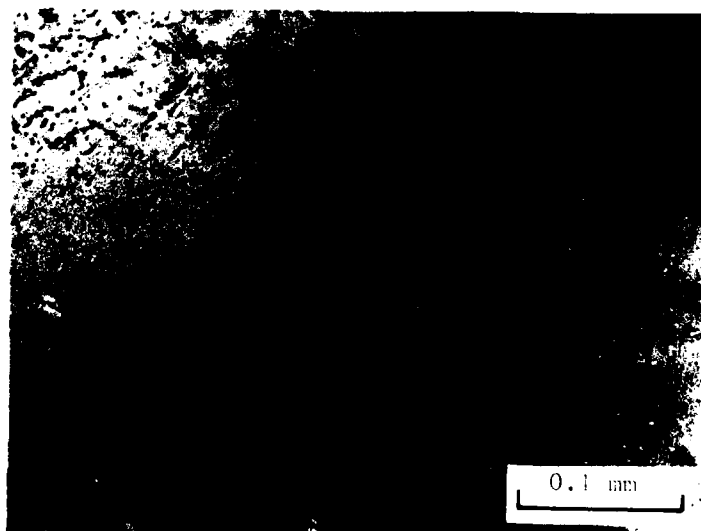
The extent of the damage in CVD MgO can be seen in the overetched region containing the impact site in Fig. 5.2. The character of this region prior to etching and the subsurface extent of the limited amount of fracture produced is shown in Fig. 5.3. The diagnostics for the water drop collision indicate excellent impact conditions were obtained. The irregularities in the general damage pattern (Fig. 5.2) are therefore due to the localized response of the grains impacted.



Figure 5.2. Overetched Impact Damage Site on CVD MgO for a 2.30 mm Water Drop Impacting at 660 ms^{-1} .



a. Reflected Light Illumination



b. Transmitted Light Illumination (Note Magnification Is Two Times that Used in the Micrograph in (a)).

Figure 5.3. Details of Damage on CVD MgO for the Water Drop Impact Shown in Figure 5.2.

The obvious experiment of introducing active dislocations into the impact surface of HP MgO was not performed due to the limited amount of material available. It is possible that plasticity initiated at induced dislocation sources may absorb some of the impact energy and reduce the extent of the fractures. It is also likely that the small grain size of this material may inhibit the plastic deformations within the surface grains from propagating very far. The stresses required to propagate slip bands from one grain to an adjacent grain may be large enough that the grain boundaries will fail first. Since the impact energy was successfully absorbed by plastic deformation in MgO for both single crystals and large grained material, it would be of interest to see which mechanism would dominate in surface abraded HP MgO. Impact energy dissipation in CVD MgO was due in part to the fact that the large grain polycrystalline material had dislocation sources distributed throughout its bulk, not just on its surface.

5.2 SPINEL

Hot-pressed spinel (MgAl_2O_4) was obtained from two different suppliers representing different starting powders and pressing schedules. Material S1 (from Ceradyne, Inc.) was processed with commercially available raw materials and was designed to have comparable mechanical properties to material S2 (from Coors Porcelain Company) even though the excellent optical clarity of S2 could not be achieved (Roy, 1981). Both of these materials included 2 w/o LiF as a sintering aid. Three additional Ceradyne materials were investigated: one with 0 w/o LiF (S0), one with 5 w/o LiF (S5), and one with 11 w/o LiF (S11) (Palicka, et al., 1979).

Both S1 and S2 had small deposits of material in their grain boundaries. The nature of these deposits can be seen in Fig. 5.4. The amorphous deposits in the grain boundaries are presumed to be compounds of LiF and MgAl_2O_4 . The assumption that the deposits are a vitreous form of LiF is supported by the dark appearance of these deposits using both secondary and back scattered electron imaging in the SEM. Both of these imaging techniques result in a darker image for materials with low atomic number relative to the background.

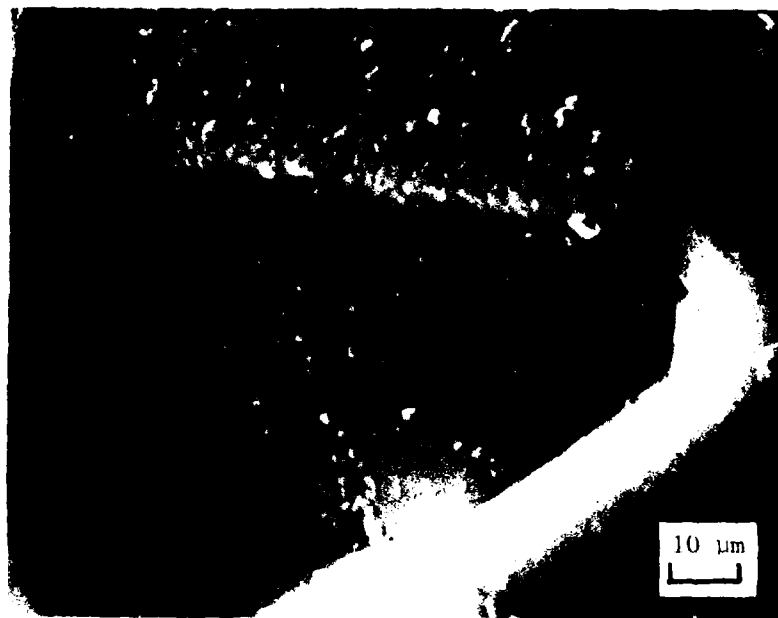
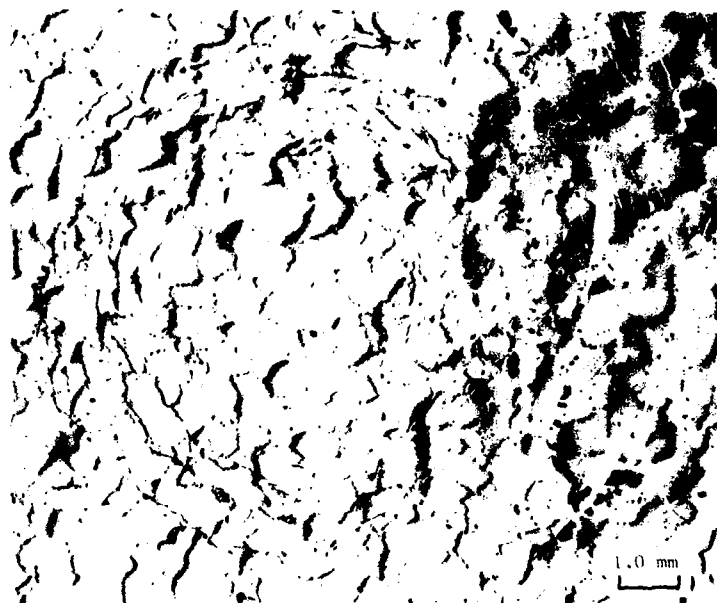


Figure 5.4. Detail of Grain Boundary Features for Spinel with 2 w/o Lithium Fluoride.

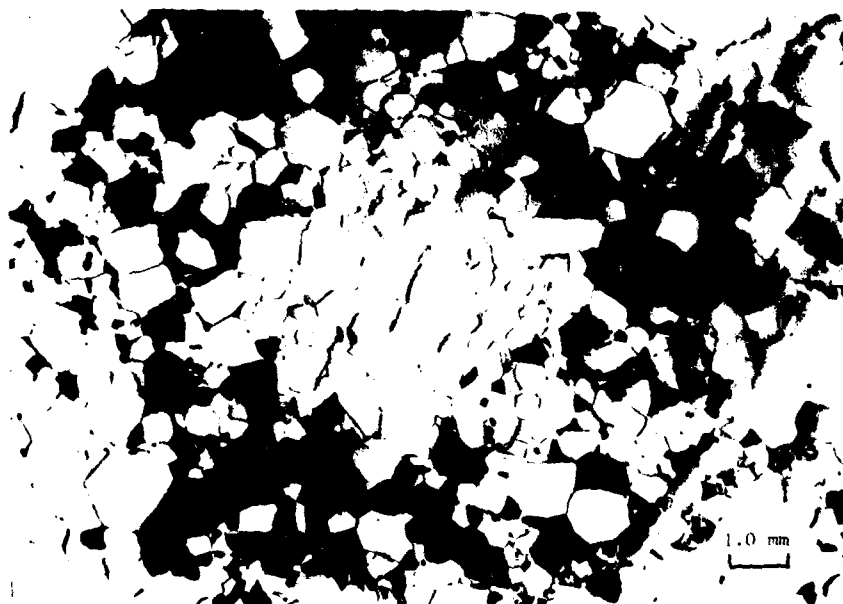
The influence of the LiF on grain boundary strength is illustrated in Fig. 5.5. For comparable impact conditions, specimen S11 exhibited a significant amount of grain removal, while the water drop impact on specimen S0 did not produce any grain removal. The fracture pattern for S0 is composed of both transgranular and intergranular fractures which results in reasonably coherent circumferential fracture arrays characteristic of finer grain materials. The grain boundary strengths appear to be comparable to the cleavage levels of the individual grains, since distribution of small fractures are seen within individual grains at the periphery of the central undamaged zone. On the other hand, the grain boundaries in S11 are extremely weak and the fractures are exclusively intergranular with easy removal of whole grains. Even at the highest velocity used for S0, 775 ms^{-1} , there was no grain removal whatsoever.

Once LiF is introduced the grain boundaries become substantially weaker, but the decreased water drop impact resistance appears to remain fairly constant as the amount of LiF is increased to in excess of 5 w/o. The extent of the damage for comparable impact conditions for materials S1, S2, and S5 are shown in Fig. 5.6. The comparison between S2 and S5 is direct. A small number of circumferential fractures are seen at large distances from the impact site for S5 in Fig. 5.6c, but otherwise the extent of the damage is comparable for S2 and S5. The additional LiF in S5 does not appear to adversely affect the grain boundary strengths beyond the strength levels for S2.

The damage comparison between S1 and S2 is not as direct, since the drop diameter was only 2.04 mm for S2 compared with 2.36 mm for S1. This means the mass of the water drop striking S1 is 1.55 times greater than the water drop impacting S2. Noting this difference in the impact conditions, it would appear that the water drop impact resistance of S2 may be comparable or only slightly superior to that of S1. Qualitatively the drop impact damage is quite similar for all three materials: the impact fractures are preferentially located in the grain boundaries over most of the damaged region.

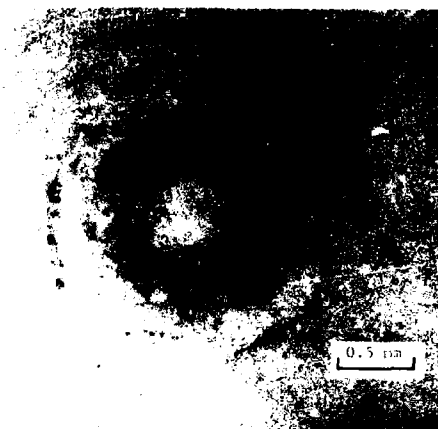
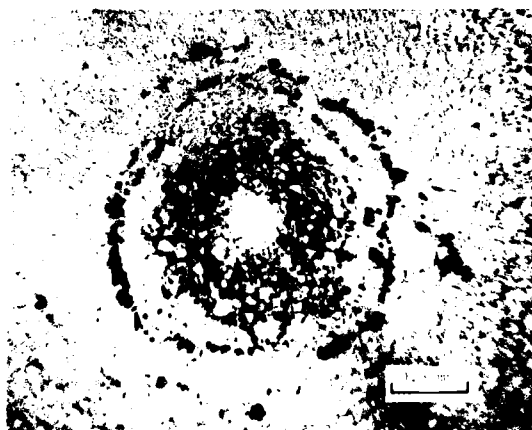


a. 2.27 mm Water Drop Impact on HP MgAl_2O_4 with 0 w/o LiF at 670 ms^{-1} .

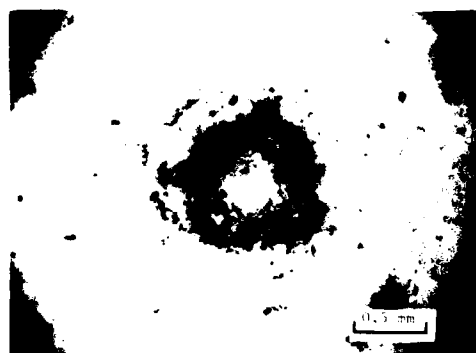
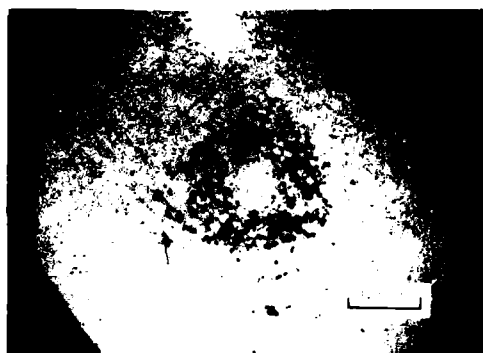


b. 2.29 mm Water Drop Impact on HP MgAl_2O_4 with 11 w/o LiF at 630 ms^{-1} .

Figure 5.5. Influence of Lithium Fluoride Content in Spinel on Water Drop Impact Damage.



a) Material S1: 2.36 mm Drop Impacting at 832 ms^{-1}



b) Material S2: 2.04 mm Drop Impacting at 826 ms^{-1}



c) Material S5: 2.10 mm Drop Impacting at 832 ms^{-1}

Figure 5.6. Comparison of Water Drop Impact Damage on Spinel Samples (Shown in Reflected and Transmitted Light Illumination).

In order to quantify the extent of the subsurface fractures in these various formulations of spinel, a significant amount of effort was devoted to preparing thin sections. Unfortunately, due to the preference of the fractures for the grain boundaries it was not possible to distinguish the fractures from the grain boundaries. What could be seen, showed the fractures followed very irregular paths, although there was a tendency to conform to the subsurface fracture pattern for ZnS.

As indicated in Section 4.5.1 it was also not possible to obtain fracture toughness values for these liquid-phase sintered materials using the indentation method, since a hemispherical indent would form beneath the Vickers indenter and grain boundaries would be opened within this region. Thus it was not possible to propagate cracks from the corners of the indenter for crack measurements to determine the fracture toughness. The quantity of material available in all cases was quite limited, so it was not possible to obtain the fracture toughness for the range of spinel formulations examined using alternative procedures. In view of the wide range of water drop impact behavior observed with LiF content, it would be interesting to determine to what extent other material and strength properties might be affected.

5.3 ALUMINA AND ALUMINA/ZIRCONIA COMPOSITES

Small samples of alumina and alumina/zirconia compositions were obtained from Dr. B. J. Hockey (National Bureau of Standards), Dr. P. F. Becher (Oak Ridge National Laboratory), and Dr. F. F. Lange (Rockwell Science Center).

The objective for this investigation was to evaluate the influence of grain size on the water drop impact resistance of alumina and to determine the effect of the zirconia toughening agent on the impact resistance in alumina/zirconia composites. The material samples received are listed in Table 5.1.

These alumina samples consisted of alumina B with an as-received grain size of 1 to 3 μm and Lucalox with a grain size of 30-50 μm . Dr. Hockey used different annealing schedules to obtain samples of alumina B

Table 5.1. Alumina and Alumina Composites.

Material	Density (kg/m^3)	E (GPa)	ν	$K_c^{1/2}$ ($\text{MPa m}^{1/2}$)	Remarks
Alumina B as received annealed 1700°C, 1 hr. annealed 1900°C, 10 min. annealed 1900°C, 1 hr. annealed 1900°C, 2 hr. annealed 1900°C, 4 hr.					Grain size 1-3 μm 3-5 μm 7.4 μm 8.4 μm 11.0 μm 13.0 μm
Lucalox					Grain size 30-50 μm
$\text{Al}_2\text{O}_3/\text{ZrO}_2$ (Becher)					ZrO_2 phase 83% tetragonal and 17% monoclinic
19 vol % ($\text{ZrO}_2 + 2 \text{ mol } \% \text{Y}_2\text{O}_3$)	3990	320	0.24	~5	
25 vol % ($\text{ZrO}_2 + 2 \text{ mol } \% \text{Y}_2\text{O}_3$)	4310	356	0.25	~8	ZrO_2 phase 75-80% tetragonal, remainder monoclinic
$\text{Al}_2\text{O}_3/\text{ZrO}_2$ (Lange)					ZrO_2 phase 100% tetragonal ZrO_2 phase 100% tetragonal ZrO_2 phase mostly tetragonal, small percentage monoclinic
20 vol % ($\text{ZrO}_2 + 2 \text{ mol } \% \text{Y}_2\text{O}_3$)					
30 vol % ($\text{ZrO}_2 + 2 \text{ mol } \% \text{Y}_2\text{O}_3$)					
40 vol % ($\text{ZrO}_2 + 2 \text{ mol } \% \text{Y}_2\text{O}_3$)					

with grain sizes ranging from 7 to 13 μm . For 2 mm water drop collisions, this grain size variation is not significant enough to differentiate the fracture interactions with the grain structure.

The materials listed in Table 5.1 were subjected to nylon bead impacts. An initial test series was carried out using a nominal 2.3 mm diameter bead impacting each specimen at 1375 ms^{-1} . This impact condition was found to be too severe. The material samples supplied by Dr. Lange were large enough that a second series of tests could be undertaken. The impact velocities ranged from 640 to 975 ms^{-1} .

Some preliminary investigations were initiated for these specimens, but as stated above the impact damage was quite severe. This effort was therefore set aside, since a significant level of effort would be required to develop suitable damage characterization procedures for these materials. The morphology of the impact fracture which have been examined is quite similar to that observed for HP MgO (Fig. 5.1).

6.0 NYLON BEAD SIMULATION OF WATER DROP IMPACTS

Adler and James (1980) demonstrated that nylon bead impacts on zinc sulfide display surface and subsurface fracture patterns which are similar to those produced by water drop collisions. As a matter of fact, the nylon bead impact damage provides a closer correspondence to water drop impact damage than that which is produced by well-characterized water jets (Field, Gorham, and Rickerby, 1979). The advantages associated with using nylon beads are greatly increased impact velocities to in excess of 4000 ms^{-1} (using ETI's capacitor discharge, particle acceleration facilities), greater flexibility in specimen geometry, and the target material can be tested at elevated temperatures as well as with the imposition of additional environmental conditions. The capacitor discharge facility maintains the advantage of a fairly rapid and simple test offered by water jets at reasonable cost.

The results from the previous experiments (Adler and James, 1980) showed an irregular fracture pattern on the surface of the specimen just outside the central undamaged zone. The intermediate to far field fracture patterns did not appear to be significantly perturbed by this effect. It was thought that the crystallinity in the nylon formation, which is unknown, used for fabricated nylon beads may be responsible for the irregular fracture pattern. In addition, these nylon beads were fairly rigid and would bounce off the surface without producing representative water drop impact damage when the impact conditions were not of sufficient intensity. Therefore an effort was undertaken to improve the quality of the nylon bead impacts.* Several different formulations of nylon suitable for making bead were obtained. These nylon formulations were selected on the basis of having more desirable properties for the water drop simulation.

* Dr. L. M. Peebles, Jr., from the Boston Branch Office of Naval Research, was most helpful in suggesting alternative nylon formulations and methods for working with the nylon flakes supplied. Dr. R. E. Phillips, Jr., Monsanto Textiles Company Technical Center, Pensacola, Florida, supplied nylon 6,6 and 6,9 and also suggested other nylon formulations which might satisfy the requirements for a suitable nylon simulation for water drop impact damages. The interest expressed by these individuals in this project is greatly appreciated.

There are several ways in which the beads could be made from the molding grade nylon received. With limited laboratory facilities available for working with polymeric materials, the number of procedures which could be pursued was limited: some procedures involved highly toxic chemicals. Nylon beads had been prepared at ETI by dropping small pieces of nylon line into a hot bath of mineral oil. A coil heater is placed near the top of a graduate. The oil is heated over a 10 cm length, while the oil in the lower portion of the cylinder is cool. The nylon segment softens in the elevated temperature portion of the column. Due to density matching of the nylon and oil and due to the temperature gradients present, the softened nylon segment will move up and down in the heated oil until it has assumed a spherical form. The spherical bead then passes out of the heated zone and slowly falls to the bottom of the graduate. After a number of beads are made the oil is cooled and strained. The beads are then collected and sorted for sphericity and uniform diameters.

This has proven to be a satisfactory procedure for very high-velocity impacts ($c.3000 \text{ ms}^{-1}$) on carbonaceous materials. However, the composition of the nylon is evident for lower velocity impacts ($c.300-600 \text{ ms}^{-1}$) on ceramic materials. These considerations therefore motivated a small developmental effort to optimize the results which could be obtained from the nylon bead simulation of water drop impact damage.

The most desirable attribute for making beads by the above procedure is that they possess a fairly sharp melting point. Nylon 11 (BMNO P40 produced by the Rilsan Corporation) had a fairly low melt temperature and melted (or softened) over a narrow temperature range. Since large bead diameters on the order of 2.5 mm were desired and due to the higher melt temperatures for the various nylons under investigation an expanded laboratory-scale operation was required. The column was now a 1 m long Pyrex tube, 5 cm inside diameter, and coil heaters were placed over a distance of 60 cm. The dwell time in the heated portion of the tube was controlled in part by the selection of several grades of silicon oil which maintained a reasonably high viscosity at elevated temperatures. The proper oil and level of heating required were optimized for nylon 11.

The flakes were also shaped into the approximate size of the beads desired which helped to produce a spherical form. The larger diameter beads often required a second pass through the heated oil column. If the various factors described above were not properly adjusted, the beads would not melt or they would assume tear-shapes. However reasonable control was achieved for nylon 11 and a quantity of acceptable beads were made for the impact experiments. Satisfactory results were not obtained with this simple arrangement for the other nylon formulations investigated: Nylon 6,6; Nylon 6,9; Trogamid T.

Nylon bead impact tests using nylon 11 (BMNO P40) on CVD zinc sulfide targets proved to be successful with respect to eliminating most of the irregularities noted in the previous test series (Adler and James, 1980). After finding that nylon 11 beads could be fabricated without too much difficulty, a supply of a super-flexible grade of nylon 11 (BMNO F25 produced by the Rilsan Corporation) was obtained and used in the subsequent evaluation program.

The advantage of using nylon beads is that they can be propelled against a stationary target. Initial impact tests were carried out in the liquid drop impact facility by suspending the nylon bead on a hair placed in the path of the sabot; the stationary bead replaces the falling water drop and the impact test procedure proceeds as usual. Since the circumferential fracture arrays were satisfactory, nylon bead impacts were undertaken using the ETI exploding wire, particle acceleration facility. A small selection of specimens from both of these test series were sectioned in order to observe the subsurface fracture patterns and to obtain the characteristic fracture measurements. The test conditions and the results from these tests are listed in Table 6.1. The fracture measurements in Table 6.1 are compared with the fracture measurements for CVD ZnS impacted by nominal 2.0 to 2.2 mm water drops in Fig. 6.1 to 6.3.

Referring to Table 6.1, the fracture measurements for Shot No. 1524 (1.74 mm diameter bead) compare quite favorably with Shot No. 1508 in Table 3.1 for a 1.90 mm water drop impacting at approximately the same

Table 6.1. Fracture Measurements for Nylon Bead Impacts on CVD ZnS

Shot No.	Impact Velocity (ms ⁻¹)	Bead Diameter (mm)	2a _c (mm)	Type I Fractures		Type II Fractures	
				Location (mm)	Depth (mm)	Location (mm)	Depth (mm)
1524	370	1.74	0.24	0.235	0.095	0.325	0.10
1525	517	1.67		Section Lost During Preparation			
1526	366	2.27	.37	.335	.23	.435	.165
1527	536	2.27	.37	.395	.58	.685	.485
E4337	354	2.27	.35	.325	.155	.46	.205
E4275	396	2.33	.49	.38	.295	.535	.29
E4339	488	2.25	.57	.485	.685	.79	.78
E4340	550	2.25	.48	.51	.445	.81	.38
E4273	550	2.37	.40	.46	.635	.91	.60
E4274	592	2.39	.45	.48	.90	1.03	.78

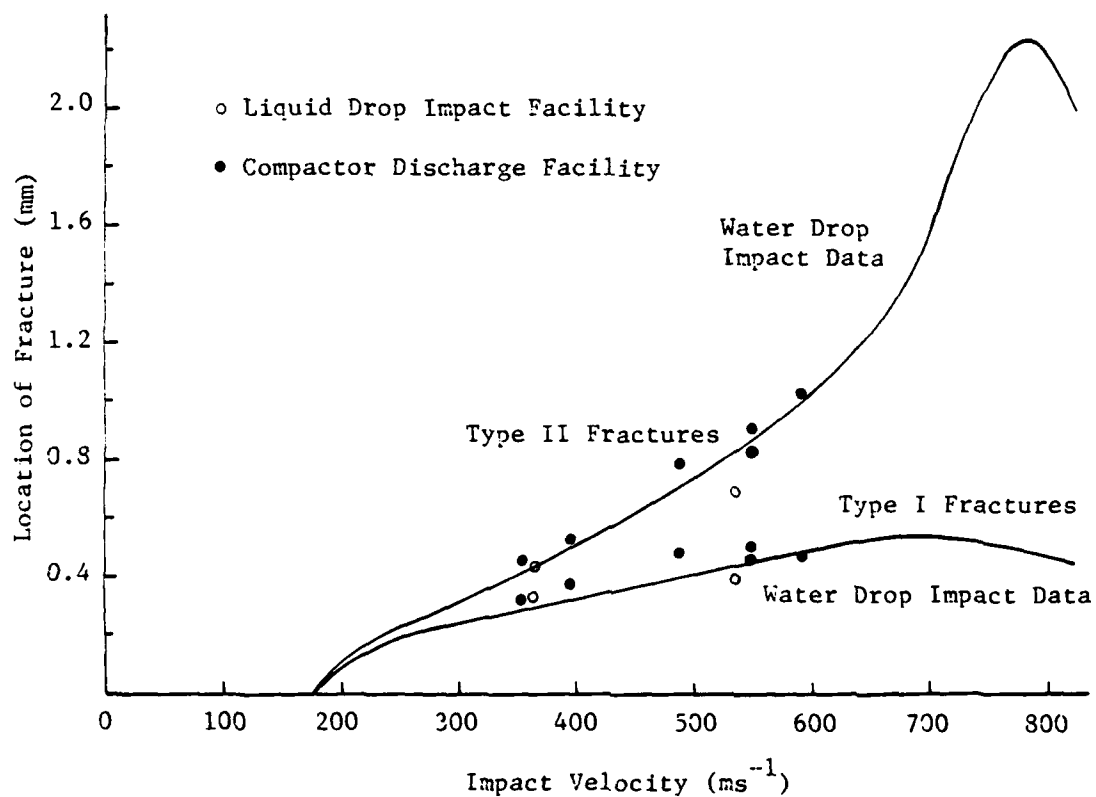


Figure 6.1. Radial Distance to Dominant Type I and Type II Fractures as a Function of Impact Velocity for Nylon Bead Impacts on CVD ZnS Compared with Water Drop Impact Data.

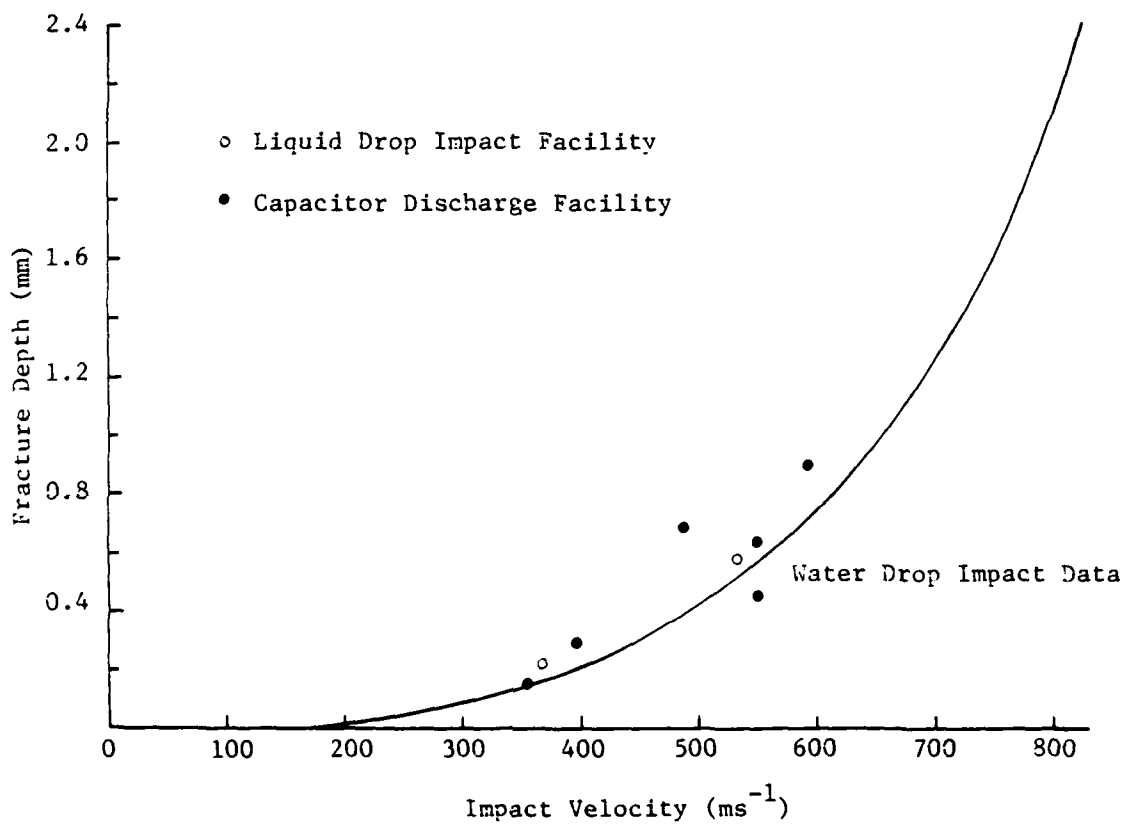


Figure 6.2. Penetration Depth for Type I Fractures as a Function of Impact Velocity for Nylon Bead Impacts on CVD ZnS Compared with Water Drop Impact Data

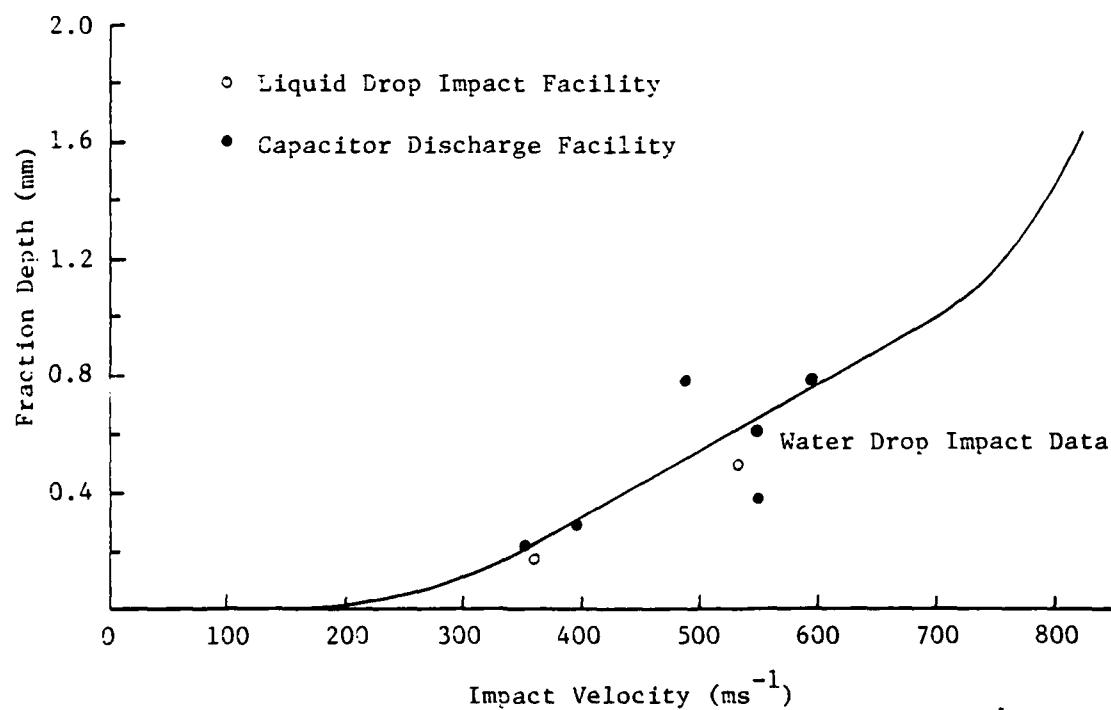


Figure 6.3. Penetration Depth for Type II Fractures as a Function of Impact Velocity for Nylon Bead Impacts on CVD ZnS Compared with Water Drop Impact Data.

velocity. The nylon impacts using the liquid drop impact facility (Shot No. 1526 and 1527) in Fig. 6.1 to 6.3 show good agreement with the water drop impact data accounting for the typical scatter inherent in these experimental results. The fracture measurements for the nylon bead impacts using the exploding wire, particle acceleration facility compare quite favorably with the water drop data. An explanation for the anomalously large fracture depth measurements for Shot No. E4339 cannot be provided; the data was reviewed but no inconsistencies could be found.

The results from the limited number of tests listed in Table 6.1 provide reasonable support for the use of nylon bead impacts as a simulation procedure for water drop impact damage. Improvements in the fracture measurement procedures, as suggested in Section 2, may help to provide a more consistent basis for these comparisons. Additional calibration of the velocity measurements for the exploding wire, particle acceleration technique in this relatively low impact velocity regime will also help to eliminate some of the experimental error in the impact velocity measurements.

7.C DISCUSSION AND CONCLUSIONS

The connection, or lack thereof, between the development of erosion-resistant materials for infrared-transmitting windows and radomes and the system requirements for aircraft and missiles was described by Adler (1979d) at the ONR Workshop on Erosion of Ceramic Materials. Some of the observations made at that time remain valid and are restated here in order to point out the technology gaps this ONR program with ETI has been addressing.

Radome materials development has been underway since World War II and the evaluation of the rain erosion behavior of a progression of various types of radome materials has also been underway for almost as long. Considerable advances have been made over the last decade in developing ceramic materials for the rigors of tactical missile applications: general handling and transportation and rapidly accelerated flight with significant dynamic loads and thermal stress gradients imposed. While the objectives for the problem of reentry vehicle erosion are well defined in terms of nosetip recession, the objectives related to the erosion of radomes are not simply stated. The work which has gone on has been directed toward evaluating the relative rain erosion damage in a variety of material candidates or toward providing direction for improving the rain erosion resistance of a particular material or class of materials. The range of mission requirements for tactical aircraft and missiles within the Department of Defense precludes that a single definition will suffice for how cumulative rain erosion damage affects the guidance systems in aircraft and missiles. The programs which have been funded have a clearly defined objective to evaluate or improve the rain erosion resistance of materials, but just how rain erosion damage in these materials influences the operation of an electronic sensor system and what level of damage can be tolerated without affecting system performance are never stated.

Several gaps were identified between the basic research effort for improving the erosion resistance of ceramic radomes to water drop impingement and the application areas where material improvements and suggestions for directions for new material development are required. It was pointed

out that rain erosion damage to tactical missiles is only one factor of several which include the thermomechanical response and electrical integrity of a radome in a severe environment, however it can be a controlling factor which limits the operational utility of an all-weather defense system. The basic research activities cannot adequately address the complexities of the combat situation, but a methodology for improving the rain erosion resistance of candidate materials, characterization of the resulting damage, and estimation of the degraded optical and electrical properties would be of considerable value. Secondly, it was noted that relatively little is known at a basic level about the nature of water drop impact damage on ceramics at velocities from 400 to 2000 ms⁻¹. This is due in part to the lack of adequate experimental facilities for conducting material-oriented research in this velocity range. Subsonic and moderate supersonic water drop collisions produce damage which in some materials is considerably more sensitive to the surface and subsurface flaws than for solid-particle impacts. Controlled experiments are therefore highly desirable since difficult-to-define a priori surface and microstructural characteristics influence the course of the resulting fractures.

Water drop impact experiments are not simply performed due to the inherent deformability of a water drop which prevents the drop from being propelled into a target as in the case of solid-particle collisions. Correspondingly, the percentage of material-oriented experiments in relation to the total testing undertaken is quite low. At present, an adequate experimental data base for materials development of ceramics for radomes and infrared-transmitting windows does not exist since

- most of the test results reported are for screening materials from an engineering viewpoint
- the impact conditions for the existing water drop impact facilities are typically estimated from circumferential evidence or are essentially unknown.
- there are relatively few detailed investigations of a single material over an extended velocity range.

The initial objective for this effort was to obtain an understanding of the response of ceramic materials on a microstructural level when subjected to water drop impact conditions (rain erosion). Before this objective could be satisfied it was necessary to have a well-controlled experimental arrangement so that the observed material damage, especially for very minor surface disruptions, could be related to a well-defined loading condition. A significant portion of the effort was devoted to achieving this test condition. The current status of the liquid drop impact facility is such that highly reproducible, well-documented, spherical water drop impacts can be obtained routinely at impact velocities from 200 to over 1000 ms^{-1} (Section 2). The diameter of the water drops at present can be varied from 1.7 to 3.3 mm (Section 3). The impact angle can range conveniently from approximately 45° to normal incidence. The capability also exists for evaluating the influence of a continuous variation in the level of water drop distortion on the extent of the damage due to distorted compared with spherical drops (Section 3). Thus, a reasonably extensive range of parameters pertaining to most aspects of water drop impingement in a flight environment now exists.

The majority of the material investigations reported during the course of this program (Adler and James, 1979, 1980, and Sections 4 and 5 of this report) utilized nominal 2.2 mm spherical drops impacting at normal incidence. A larger drop diameter is used for very high strength ceramics in order to provide an impact condition that is severe enough to produce measurable damage. Detailed investigations of calcium fluoride (Adler and James, 1979), magnesium oxide (Adler and James, 1979; this report), lithium fluoride (Adler and James, 1979), magnesium aluminate spinel (this report), and zinc sulfide (Adler and James, 1980; this report) were undertaken. In addition polymethylmethacrylate was used to obtain information about the impact loading conditions (Adler and James, 1979). Due to the excellent water drop impacts which can be obtained in the liquid drop impact facility, the development of adequate surface finishing procedures, and the development of damage characterization procedures, the results reported in previous investigations on lithium fluoride, zinc sulfide, and polymethylmethacrylate were shown to be completely in error or inaccurate. (Reference should be made to the respective reports for accounts of these investigations).

In order to relate the impact damage to material properties a selection of materials for which the material properties are reasonably well known was finally assembled. The extent of the water drop impact damage was estimated from the surface fractures produced by roughly equivalent impact conditions (see Section 4). This comparison indicates that it is quite difficult to impossible to establish the water drop impact resistance of ceramic materials from their conventionally measured material properties. The water drop impact resistance displays wide variations for materials with essentially similar material properties. More detailed investigations are required to determine if any universal material properties can be found which control the water drop impact resistance of ceramic materials. With carefully planned experiments and specially prepared materials this objective can at last be adequately addressed based on the work accomplished within this program.

The comparison between actual water drop impacts and simulations of water drop impacts (water jets and soft solid particle impacts) has quantified the similarities and differences in the superficially similarly appearing damage for each test condition (Adler and James, 1980; this report). Impacts produced by the proper formulation of nylon were shown to be much more representative of water drop impacts than water jets. This finding can now be refined and utilized as a practical means for simulating water drop impact conditions that would be quite difficult and costly to do with actual water drops, such as, elevated temperature impact tests and residual strength evaluations of full-scale components.

The work accomplished during the course of this investigation has contributed to clarifying prior concepts of rain erosion damage in materials, has provided a basis for the analysis of water drop impact damage and erosion predictions, has demonstrated that the suggested correlations between water drop impact damage and material properties cannot be substantiated, has provided a consistent means for experimentally evaluating the water drop impact resistance of materials, and has generated an alternative means (nylon bead impacts) for obtaining water drop impact damage evaluations for actual components, for superposed

thermal environments, and for an extended range of impact velocities. Rapid progress should now be made in understanding and predicting rain erosion damage in materials utilizing these accomplishments which have required a considerable amount of time and effort to reach their present stage of development.

References

- W.F. Adler (1979a). "Particulate Erosion of Electromagnetic Window Materials," Optical Engineering, 18, 610-619.
- W.F. Adler (1979b). "The Mechanics of Liquid Impact," Treatise on Materials Science and Technology, Vol 16 (C.M. Preece, editor), New York: Academic Press, 127-183.
- W.F. Adler (1979c). "Single Water Drop Impacts on Polymethylmethacrylate," Proc. Fifth Int. Conf. on Erosion by Solid and Liquid Impact (September 1979).
- W.F. Adler (1979d). "Discussion of Rain Erosion Research Activities," Summary of Office of Naval Research Workshop on Erosion of Ceramic Materials (R.C. Pohanka, editor), (26,27 June 1979), 41-51.
- W.F. Adler (1981). "Development of Design Data for Rain Impact Damage in Infrared-Transmitting Materials," Proceedings of the Society of Photo-Optical Instrumentation Engineers, Vol. 297, Emerging Optical Materials (S. Musikant, editor), 143-154.
- W.F. Adler, J.C. Botke, and T.W. James (1979). Response of Infrared Materials to Raindrop Impact, AFML-TR-79-4151 (October 1979).
- W.F. Adler and S.V. Hooker (1977). Impact Damage in Single Crystals, Technical Report for Office of Naval Research, Contract No. N00014-76-C-0744 (July 1977).
- W.F. Adler and S.V. Hooker (1978). "Water Drop Impact Damage in Zinc Sulfide," Wear, 48, 103-119.
- W.F. Adler and T.W. James (1979). Particle Impact Damage in Ceramics, Technical Report for Office of Naval Research Contract No. N00014-76-C-0744 (March 1979)
- W.F. Adler and T.W. James (1980). Localized Deformation and Fracture of Transparent Ceramics, ONR Technical Report for Contract No. N00014-76-C-0744 (March 1980).
- A. Behrendt (1974). "Study of Parameters of Flight Materials at Speeds up to 1000 Meters per Second," Proc. Fourth Int. Conf. on Rain Erosion and Associated Phenomena, (A.A. Fyall, and R.B. King, eds.), Royal Aircraft Establishment, Farnborough, England, 425-448.
- J.H. Brunton and M.C. Rochester (1979). "Erosion of Solid Surface by the Impact of Liquid Drops," in Treatise on Materials Science and Technology, Vol. 16 (C.M. Preece, ed.), New York: Academic Press, 186-248.
- A.G. Evans (1979). Personal Communication.
- A.G. Evans (1982a). Fracture toughness determined for CVD ZnS, HP ZnS, and CVD ZnSe used in this program.

- A.G. Evans (1982b). Personal Communication: results from unpublished work.
- A.G. Evans and E.A. Charles (1976). "Fracture Toughness Determinations by Indentation," J. Amer. Ceramic Soc., 59, 371-372.
- A.G. Evans, Y.M. Ito, and M. Rosenblatt (1980). "Impact Damage Thresholds in Brittle Materials Impacted by Water Drops," J. Appl. Phys., 51, 2473-2482.
- A.G. Evans and H. Johnson (1975). "A Fracture-Mechanics Study of ZnSe for Laser Window Applications," J. Amer. Ceramics Soc., 58, 244-249.
- A.G. Evans and T.R. Wilshaw (1976). "Quasi-Static Solid Particle Damage in Brittle Solids - I. Observations, Analysis, and Implications," Acta Met., 24, 939-956.
- J.E. Field, D.A. Gorham, and D.G. Rickerby (1979). "High-Speed Liquid Jet and Drop Impact on Brittle Targets," Erosion: Prevention and Useful Applications, ASTM STP 664. (W.F. Adler, editor), American Society for Testing and Materials, 1979, 298-319.
- S.W. Freiman, J.J. Mecholsky, Jr., R.W. Rice, and J.C. Wurst (1975). "Influence on Crack Propagation in ZnSe," J. Amer. Ceramic Soc., 58, 406-409.
- S.V. Hackworth and L.H. Kocher (1978). Behavior of Infrared Window Materials Exposed to Rain Drop Environments at Velocities to 2000 FPS (610 M/S), AFML-TR-78-184 (September 1978).
- R.G. Hoagland and R.G. Jung (1978). Water-Droplet Impact-Characterization of Damage Mechanisms, Office of Naval Research Final Technical Report for Contract No. N00014-76-C-0645.
- S.V. Hooker and W.V. Adler (1978). "Particle Impact Regimes in Single Crystals," Fracture Mechanics of Ceramics, Vol. 3 (R.C. Bradt, D.P.H. Hasselman, and F.F. Lange, editors), New York: Plenum Press, 333-347.
- K.H. Jolliffe (1966). "The Application of Dislocation Etching Techniques to the Study of Liquid Impacts," Phil. Trans., A260, 101-108.
- H.P. Kirchener (1981). Personal Communication.
- J.L. Lankford and R.A. Leverance (1971). Determination of Threshold Damage in Radome Materials by Discrete Impact in a Ballistics Range, Naval Ordnance Laboratory Technical Report NOLTR-71-113.
- J.L. Lankford, R.A. Leverance, and S.A. Longas (1973). Threshold Damage in Radome Materials by Discrete Water Impact (Ballistics Range Investigation), Naval Ordnance Laboratory Report NOLTR-73-34.

- S. Musikant, R.A. Tanzilli, H. Rauch, S. Prochazka, and S.C. Huseby (1980). "Advanced Optical Ceramics - Phase I," Proceedings of the Fifteenth Symposium on Electromagnetic Windows (H.L. Barrett and G.K. Huddleston, ed.), Atlanta, GA: Georgia Institute of Technology.
- R.J. Palicka, J.A. Rubin, and F.S. Valent (1979). Development of Optically Transparent Hot Pressed Spinel (MgAl_2O_4). Final Report for Naval Weapons Center Contract No. N60530-77-C-0079 (September 1979).
- A.A. Ranger and J.A. Nicholls (1969). "Aerodynamic Shattering of Liquid Drops," AIAA J., 7, 285-290.
- R.W. Rice, S.W. Freiman, R.C. Pohanka, J.J. Mecholsky, Jr., and C. Cm. Wu (1978). "Microstructural Dependence of Fracture Mechanics in Ceramics," Fracture Mechanics of Ceramics, Vol. 4 (R.C. Bradt, D.P.H. Hasselman, and F.F. Lange, editors), New York: Plenum Press, 849-876.
- M. Rosenblatt, Y.M. Ito, and G.E. Eggum (1979). "Analysis of Brittle Target Fracture from a Subsonic Water Drop Impact," Erosion: Prevention and Useful Applications, ASTM STP 664 (W.F. Adler, ed.), American Society for Testing and Materials, 227-254.
- D.W. Roy (1981). Development of Hot-Pressed Spinel for Multispectral Windows and Domes, AFWAL-TR-81-4005 (March 1981).
- D.A. Schockey, D.J. Rowcliffe, and K.C. Dao (1977). "Fracture Toughness of CVD ZnS," Topical Report for Office of Naval Research Contract N00014-76-C-0657 (March, 1977).
- R.L. Stewart and R.C. Bradt (1980a). "Fracture of Single Crystal MgAl_2O_4 ," J. Materials Sci., 15, 67-72.
- R.L. Stewart and R.C. Bradt (1980b). "Fracture of Polycrystalline MgAl_2O_4 ," J. Amer. Ceramic Soc., 63, 619-623.
- R.L. Stewart, M. Iwasa, and R.C. Bradt (1981). "Room Temperature K_{Ic} Values for Single Crystal and Polycrystalline MgAl_2O_4 ," J. Amer. Ceramic Soc., 64, C-22 to C-23.
- S. van der Zwaag, J.T. Hagan, and J.E. Field (1980). "Studies of Contact Damage in Polycrystalline Zinc Sulphide," J. Materials Sci., 15, 2965-2972.
- G.D. Waldman, W.G. Reinecke, and D.C. Glenn (1972). "Raindrop Breakup in the Shock Layer of a High Speed Vehicle," AIAA J., 10, 1200-1204.
- J.M. Wimmer and G.A. Graves (1977). Exploratory Development of Multidisciplinary Characterization of Infrared Transmitting Materials, Semi-annual Progress Report No. 1 for AFML Contract No. F33615-77-C-5004, UDRI-TR-77-35 (July 1977).
- J.M. Wimmer and G.A. Graves (1978a). Exploratory Development of Multidisciplinary Characterization of Infrared Transmitting Materials, Semiannual Progress Report No. 2 for AFML Contract No. F33615-77-C-5004, UDRI-TR-77-35 (February 1978).

J.M. Wimmer and G.A. Graves (1978b). Exploratory Development of Multidisciplinary Characterization of Infrared Transmitting Materials, Semiannual Progress Report No. 3 for AFML Contract No. F33615-77-C-5004, UDRI-TR-77-35 (August 1978).

J.C. Wurst and T.P. Graham (1976). Thermal, Electrical and Physical Measurements of Laser Window Materials, AFML-TR-75-28 (April 1975).

Technical Reports for Contract No. N00014-76-C-0744

W.F. Adler and S.V. Hooker, Impact Damage in Single Crystals, (July 1977).

W.F. Adler and T.W. James, Particle Impact Damage in Ceramics, (March 1979).

W.F. Adler and T.W. James, Localized Deformation and Fracture of Transparent Ceramics, (March 1980).

Publications from Contract No. N00014-76-C-0744

- W.F. Adler, "Rain Erosion Mechanisms for Optical Materials," Society of Photo-Optical Instrumentation Engineers, Vol. 121, Optics in Adverse Environments, (1978), 19-37.
- S.V. Hooker and W.F. Adler, "Particle Impact Regimes in Single Crystals," Fracture Mechanics of Ceramics, Volume 3 (R.C. Bradt, D.P.H. Hasselman, and F.F. Lange, editors), New York: Plenum Press, 1978, 333-347.
- W.F. Adler, "The Mechanics of Liquid Impact," Treatise on Materials Science and Technology, Vol. 16 (C.M. Preece, editor), New York: Academic Press, 1979, 127-183.
- W.F. Adler, "Single Water Drop Impacts on Polymethylmethacrylate," Proc. Fifth Int. Conf. on Erosion by Solid and Liquid Impact (September 1979).
- W.F. Adler, "Particulate Erosion of Electromagnetic Window Materials," Optical Engineering, 18 (1979), 610-619.
- W.F. Adler, Editor, Erosion: Prevention and Useful Applications, ASTM STP 664, Philadelphia: American Society for Testing and Materials, 1979.
- W.F. Adler and T.W. James, "Localized Deformation and Fracture of Magnesium Oxide," Fractography and Materials Science, ASTM STP 733 (L.N. Gilbertson and R.D. Zipp, ed.), American Society for Testing and Materials, 1981, 271-290.
- W.F. Adler and T.W. James, "Analysis of Water Impacts on Zinc Sulfide," to be published in the Proceedings of the Third Symposium on Fracture Mechanics of Ceramics.
- W. F. Adler, "Material Property Correlations for Water Drop Impact Damage in Electromagnetic Window Materials," to be published in the Proceedings of the Sixteenth Symposium on Electromagnetic Windows.
- W.F. Adler, "Influence of Water Drop Distortion on Impact Damage," to be published in the Proceedings of the Sixteenth Symposium on Electromagnetic Windows.
- W.F. Adler, "Degradation of Optical Materials Exposed to Water Drop Impacts," to be published in the Proceedings of the Society of Photo-Optical Instrumentation Engineers, Scattering in Optical Materials.